Title

Combined Experimental and Theoretical Study on the Formation of the Elusive 2-Methyl-1-silacycloprop-2-enylidene Molecule under Single Collision Conditions via Reactions of the Silylidyne Radical (SiH; X2Π) with Allene (H2CCCH2; X1A1) and D4-Allene (...

Permalink
https://escholarship.org/uc/item/82n2q905

Journal
The Journal of Physical Chemistry A, 119(50)

ISSN
1089-5639

Authors
Yang, Tao
Dangi, Beni B
Maksyutenko, Pavlo
et al.

Publication Date
2015-12-17

DOI
10.1021/acs.jpca.5b09773

Peer reviewed

A Combined Experimental and Theoretical Study on the Formation of the Elusive 2-Methyl-1-silacycloprop-2-enylidene Molecule under Single Collision Conditions via Reactions of the Silylidyne Radical (SiH; $X^2\Pi$) with Allene (H_2CCCH_2; X^1A_1) and D4-Allene (D_2CCCD_2; X^1A_1)

Journal:	*The Journal of Physical Chemistry*
Manuscript ID	jp-2015-09773w.R1
Manuscript Type:	Special Issue Article
Date Submitted by the Author:	03-Nov-2015
Complete List of Authors:	Yang, Tao; University of Hawai'i at Manoa, Chemistry Department, Dangi, Beni; University of Hawai'i at Manoa, Chemistry Department, Maksyutenko, Pavlo; University of Hawai'i at Manoa, Chemistry Department, Kaiser, Ralf; University of Hawai'i at Manoa, Chemistry Department, Bertels, Luke; University of California, Berkeley, Chemistry Department, Head-Gordon, Martin; University of California, Berkeley, Chemistry Department,

A Combined Experimental and Theoretical Study on the Formation of the Elusive 2-Methyl-1-silacycloprop-2-enylidene Molecule under Single Collision Conditions via Reactions of the Silylidyne Radical (SiH; $X^2\Pi$) with Allene (H_2CCCH_2; X^1A_1) and D4-Allene (D_2CCCD_2; X^1A_1)

Tao Yang, Beni B. Dangi, Pavlo Maksyutenko, Ralf I. Kaiser*

Department of Chemistry, University of Hawai'i at Manoa, Honolulu HI 96822

Luke W. Bertels, Martin Head-Gordon*

Department of Chemistry, University of California, Berkeley, Berkeley CA 94720

Corresponding Authors:

Professor Dr. Ralf I. Kaiser; Email: ralfk@hawaii.edu; Phone: +1-808-956-5731

Professor Dr. Martin Head-Gordon; Email: mhg@cchem.berkeley.edu; Phone: +1-510-642-5957

ABSTRACT

The crossed molecular beam reactions of the ground state silylidyne radical (SiH; $X^2\Pi$) with allene (H_2CCCH_2; X^1A_1) and D4-allene (D_2CCCD_2; X^1A_1) were carried out at collision energies of 30 kJ mol^{-1}. Electronic structure calculations propose that the reaction of silylidyne with allene has no entrance barrier and is initiated by silylidyne addition to the π electron density of allene either to one carbon atom (C1/C2) or to both carbon atoms simultaneously via indirect (complex forming) reaction dynamics. The initially formed addition complexes isomerize via *two distinct reaction pathways* leading eventually both to a cyclic SiC_3H_5 intermediate. The latter decomposes through a loose exit transition state via an atomic hydrogen loss perpendicularly to the plane of the decomposing complex (sideways scattering) in an overall exoergic reaction (experimentally: - 19 ± 13 kJ mol^{-1}; computationally: - 5 ± 3 kJ mol^{-1}). This hydrogen loss yields the hitherto elusive 2-methyl-1-silacycloprop-2-enylidene molecule (c-SiC_3H_4), which can be derived from the closed shell cyclopropenylidene molecule (c-C_3H_2) by replacing a hydrogen atom with a methyl group and the carbene carbon atom by the isovalent silicon atom. The synthesis of the 2-methyl-1-silacycloprop-2-enylidene molecule in the bimolecular gas phase reaction of silylidyne with allene enriches our understanding toward the formation of organosilicon species in the gas phase of the interstellar medium in particular via exoergic reactions of no entrance barrier. This facile route to 2-methyl-1-silacycloprop-2-enylidene via a silylidyne radical reaction with allene opens up a versatile approach to form hitherto poorly characterized silicon-bearing species in extraterrestrial environments; this reaction class might represent the missing link leading from silicon-bearing radicals via organosilicon chemistry eventually to silicon-carbon-rich interstellar grains even in cold molecular clouds where temperatures are as low as 10 K.

1. Introduction

The energetics and dynamics of elementary reactions of the simplest silicon-bearing radical – silylidyne ($SiH(X^2\Pi)$) – with prototype hydrocarbon molecules under single collision conditions is of crucial interest to understand the formation of organosilicon molecules both from the experimental and theoretical viewpoints spanning astrochemistry and physical organic chemistry. First, considering the astrochemical relevance, an understanding of the chemical reaction dynamics of silylidyne with prototype hydrocarbon molecules is necessary to reveal the underlying molecular processes involved in the formation of organosilicon molecules in the interstellar medium.[1-4] This is due to the key role of silicon-bearing molecules in the formation of silicon carbide dust grains in the outflow of circumstellar envelopes of carbon rich Asymptotic Giant Branch (AGB) stars like IRC+10216,[5-14] which may account for up to 80 % of the silicon abundance in the interstellar medium bound to carbon.[15-17] However, with temperatures rising up to a few 1,000 K close to the photosphere of the central star,[18] the basic molecular processes, which link the circumstellar silicon and carbon chemistries to dust formation, are far from being understood.[19-21] Astrochemical models proposed that the formation of organosilicon molecules are driven by reactions of small silicon-bearing radicals such as silylidyne with hydrocarbon molecules,[2, 22-24] involving atomic and/or molecular hydrogen replacement channels (reactions (1) and (2), respectively). Silylidyne radicals are predicted to be present at fractional abundances of up to 2×10^{-7} within two stellar radii of IRC+10216,[25] however, the chemical dynamics of these reactions with key hydrocarbon molecules have not been explored yet.

(1) $$SiH + C_xH_y \rightarrow SiC_xH_y + H,$$

(2) $$SiH + C_xH_y \rightarrow SiC_xH_{y-1} + H_2.$$

These considerations have led to the development of astrochemical models of, for instance, the circumstellar organosilicon chemistry of the bright carbon star IRC+10216. Nevertheless, astrochemical models show inconsistent growth mechanisms for the principal routes to the build-up of organosilicon molecules in the interstellar medium. For instance, calculated column densities of silicon carbide (SiC) and silicon dicarbide (c-SiC_2) are diverged by up to a factor of three from observed values.[16] This disagreement is based on inaccurate laboratory data such as product branching ratios and incorrect thermochemistry of the neutral-neutral reactions of silylidyne radicals with hydrocarbon molecules.[26-27] Based on these shortcomings, Ziurys called explicitly for a systematic experimental study on the formation and chemical bonding of (hydrogenated) silicon carbides via reactions of silicon bearing species.[15, 28-30] Likewise, Millar et al. reiterated that experimental studies on reactions of silicon-bearing radicals are imperative, stressing that the products of silylidyne radical reactions are completely unknown and that the branching ratios are simply guessed – a crucial limitation of these models.[31-34] In preliminary models, Howe and Millar proposed key neutral-neutral reaction mechanisms aiming to rationalize the formation of silicon-carbide clusters in the outflow of the envelopes.[35] On the other hand, Gensheimer et al. proposed that the formation of silicon dicarbide (c-SiC_2) involves hitherto unstudied ion-molecule reactions with acetylene (C_2H_2) acting as the progenitor.[36] However, the penetration of the interstellar ultraviolet field has been limited thus failing to produce ionized species in the inner shell of IRC+10216. Therefore, MacKay and Charnley confirmed the necessity of incorporating neutral-neutral reactions pointing out that silane (SiH_4) might represent a precursor to the silylidyne radical.[16] Willacy and Cherchneff demonstrated nicely that in the region of thermal equilibrium, the silylidyne radicals have significant fractional abundances of up to 2×10^{-7},[25] which is three orders of magnitude higher than the silylene (SiH_2; 1×10^{-10}). Based on these considerations, Wakelam,[23] Ziurys,[15, 30] Millar,[2, 29] and Kaiser[37, 38] et al. emphasized the need of the involvement of silicon-bearing molecules and the connection of the silicon with the circumstellar carbon chemistry. Therefore, if we determine the chemical dynamics of silylidyne radical ($SiH(X^2\Pi)$) reactions with key hydrocarbon molecules, we will eliminate these central uncertainties and provide well-constrained information on the reaction products (organosilicon molecules) and their branching ratios – crucial data to rationalize the interstellar organosilicon chemistry.

Second, organosilicon molecules have attracted substantial interest from the physical organic chemistry community to better understand basic concepts of molecular structure and chemical bonding of carbon versus silicon.[8, 39-51] Although silicon and carbon belong to the same main group and hence are isovalent, the chemical bonding of carbon versus silicon is quite distinct. This is well demonstrated by the structure of the cyclic C_{2v} symmetric c-SiC_2 molecule, while the tricarbon (C_3) molecule is linear. Likewise, isovalent cyano (CN) and silicon nitride (SiN) radicals have discrete reactivities with acetylene and ethylene leading to nitriles (HCCCN, C_2H_3CN)[52-55] and isosilacyano products (HCCNSi, C_2H_3NSi),[55-57] respectively. A replacement of a carbon by an isovalent silicon atom may lead to novel molecules, whose carbon-analog counterparts do not exist. So far, theses aspects of the organosilicon chemistry and the formation of chemical bonds involving silicon are not well understood.

Since the first synthesis and characterization of the silicon-carbon double bond in 1,1,2-trimethylsilaethylene ($(CH_3)_3SiCH$) in 1976,[58] increasing interest has been devoted to strained and unsaturated organosilicon compounds. Gordon et al. conducted ab initio calculations at the 6-31G* and 3-21G* levels on selected SiC_3H_4 isomers and identified 10 cyclic structures and 8 acyclic isomers with the global minimum proposed to be 2-methyl-l-silacycloprop-2-en-l-ylidene (6) (Figure 1).[59-61] Further, 4-silatriafulvene (SiC_3H_4) was proposed to hold a nonplanar C_s symmetry due to the aromatic character of the ring system.[62-63] This is in strong contrast to methylenecyclopropene (c-C_4H_4) which is C_{2v} symmetric. The intrinsic polarity of the Si=C bond in 4-sliatriafulvene aroused substantial interest from the synthetic organic chemistry community leading to the first synthesis of isolable 4-silatriafulvene more than a decade after Gordon's studies.[64-65] Further, enlightened by facile chemisportion of cycloalkenes on metal surfaces, Gentle and Muetterties synthesized silacyclobutane (SiC_3H_8) and silacyclobutadiene (SiC_3H_4) on a Pd(110) surface via thermal desorption.[66] Fink et al. generated silacyclobutadiene in hydro-carbon glass at 77 K via a photochemical rearrangement of cyclopropenylsilylene;[67] Puranik compiled detailed synthetic routes leading to silacylcobutadiene.[68]

Despite the key role of small organosilicon molecules in understanding basic concepts of chemical bonding compared to their isoelectronic hydrocarbon counterparts, and in rationalizing the role of silicon-bearing molecules in interstellar environments such as in circumstellar envelopes of carbon stars like IRC+10216, the fundamental question, how these silicon-bearing molecules are formed, has not been answered. Likewise, an experimental and theoretical investigation of the related potential energy surfaces is still in its infancy. The only studies under single collision conditions have been limited to the atomic silicon – acetylene[37] and silylidyne – acetylene systems[38] leading to the linear ethynylsilylidyne radical (SiCCH) and to silacyclopropenylidene (c-SiC_2H_2) via atomic hydrogen loss in single collision events. Here, the elucidation of reaction mechanisms involving organosilicon molecules and a comparison with the corresponding carbon analog systems under single collision conditions can help to shed light not only on the distinct reactivity of ground state silylidyne ($SiH(X^2\Pi)$) versus methylidyne radicals ($CH(X^2\Pi)$), but also on the molecular structures and chemical bonding of hitherto elusive molecules within the SiC_xH_y (x≤6, y≤6) systems. This comparison of the chemical behavior of silicon relative to carbon will have a crucial impact in rationalizing chemical bonding involving silicon atoms and how we think about chemical structure. Here, we expand on our knowledge of the formation of small organosilicon molecules under single collision conditions, and present the results of a combined experimental and theoretical investigation of the reaction of the ground state silylidyne (SiH; $X^2\Pi$) with allene (H_2CCCH_2; X^1A_1).

2. Experimental Methods

The crossed beam reactions of the silylidyne radical (SiH; $X^2\Pi$) with allene (H_2CCCH_2; X^1A_1) and with D4-allene (D_2CCCD_2; X^1A_1) were conducted in a universal crossed molecular beams machine under single collision conditions.[69-73] We generated a pulsed supersonic beam of ground state silylidyne radical (SiH; $X^2\Pi$) via the photolysis of disilane (Si_2H_6; 99.998 %; Voltaix) seeded in helium (He; 99.9999 %; Gaspro) at a seeding fraction of 0.5 %. This mixture was fed into a pulsed piezoelectric valve (Piezo Disk Translator P-286.23; Physik Instrumente) operating at a repetition rate of 120 Hz, pulse width of 80 μs, a peak voltage of -400 V, and 1,520 Torr backing pressure, before introducing the mixture into the primary source chamber. Since disilane has a flammability limit as low as 0.2 % in air, we incorporated a liquid nitrogen cooled cold trap (Nor-Cal products) in the foreline between the turbomolecular pump and the backing pump station to trap the non-photolyzed disilane. The output of an excimer laser (ArF, 193 nm, 30 mJ per pulse) was focused with a UV-coated lens of 2 meter focal length; this output intercepted the molecular beam 2 mm downstream of the nozzle over a spot area of 1 mm × 4 mm. Recent laboratory studies determined the photodissociation cross section of disilane leading to silylidyne radicals to be 5×10^{-18} cm^2.[74] Accounting for the pulse energy and the laser spot size in the photodissociation region, our 193 nm photon flux of 7×10^{17} cm^{-2} per pulse is sufficiently high enough to reach saturation level. The pulsed beam of the silylidyne radicals passed through a skimmer; a four-slit chopper wheel rotating at 120 Hz selected a section of this beam with a well-defined peak velocity (v_p) and speed ratio (S) of 1730 ± 13 m s^{-1} and 18.9 ± 2.9, respectively. Based on calibration experiments with helium, neon and argon, we determined number densities of a few 10^{12} radicals cm^{-3} per laser pulse in the interaction region of the scattering chamber.[75] In the interaction region, this pulse intercepted the most intense part of a pulsed allene/D4-allene beam (C_3H_4, Organic Technologies; C_3D_4, CDN Isotopes) held at a backing pressure of 550 Torr perpendicularly. Peak velocities (v_p) and speed ratios (S) for the secondary beam were determined to be 800 ± 10 ms^{-1} and 12.0 ± 0.4, and 790 ± 10 ms^{-1} and 12.0 ± 0.4, respectively. This yields nominal collision energies of 30.3 ± 0.7 kJ mol^{-1} and 31.4 ± 1.0 kJ mol^{-1} as well as center-of-mass angles of $32.5 \pm 0.6^{\circ}$ and $34.6 \pm 0.6^{\circ}$, respectively. Note that the primary pulsed valve was triggered 1886 μs after the time zero defined by the infrared diode mounted on top of the chopper wheel; since the secondary beam was slower than the primary beam, the secondary pulsed valve was triggered 37 μs prior to the primary one to allow a maximum overlap in the interaction region. Finally, the excimer laser was triggered 155 μs after the primary pulsed valve to guarantee an efficient overlap of the gas pulse with the laser beam. To allow a 'laser-off' minus 'laser-on' background subtraction, both valves were triggered at 120 Hz, but the laser was operated at 60 Hz. The pulse sequence of the experiments is shown in Figure 2.

It is important to highlight that we determined the velocity and the speed ratio of the silylidyne radical beam on-axis in the time-of-flight (TOF) mode. Since signal at $m/z = 29$ (SiH^+) also originates from dissociative ionization of non-photolyzed disilane in the ionizer, even a *laser on* minus *laser off* subtraction at 80 eV electron impact energy cannot fully eliminate this contribution. Therefore, we operated the electron impact ionizer in the *soft ionization* mode at an electron energy of 26 eV. This allowed sufficient signal from ionization of the silylidyne radical, but greatly reduced signal from dissociative ionization of the disilane precursor.[37] Here, the TOF spectra of the silylidyne beam were obtained at an electron energy of 26 eV with an emission current of 1 mA and a calibrated ion-flight constant of 3.75 ± 0.13 μs amu$^{-1/2}$ at 26 eV; in contrast, this ion flight constant is lower than those obtained at 34 eV (3.85 μs amu$^{-1/2}$) and 80 eV (5.25 μs amu$^{-1/2}$).

The reactively scattered products were then mass filtered exploiting a quadrupole mass spectrometer (QMS) operated in the TOF mode and a Daly ion detector housed in a rotatable, triply-differentially pumped ultrahigh vacuum chamber after electron-impact ionization of the neutral products at an electron energy of 80 eV and an emission current of 2 mA. The detector can be rotated within the plane defined by the primary and the secondary reactant beams to collect angular resolved TOF spectra. At each angle, up to 6×10^5 TOF spectra were accumulated to obtain good signal-to-noise ratios. Filtered by the Extrel QC 150 quadruple mass spectrometer at 1.2 MHz, the ions of a well-defined mass-to-charge (*m/z*) ratio were directed toward a stainless steel target coated with a thin aluminum layer floated at -22.5 kV. Triggered by the impact of the cations on the aluminum coated stainless steel target, an electron cascade is generated and accelerated onto an aluminum-coated organic scintillator to initiate a photon pulse which is further amplified by a photomultiplier tube (PMT, Burle, Model 8850) operating at -1.35 kV. The signal was filtered by a discriminator (Advanced Research Instruments, Model F-100TD) at a discrimination level of 1.6 mV and fed into a Stanford Research System SR430 multichannel scaler. The recorded TOF spectra were then integrated and normalized to extract the product angular distribution in the laboratory frame. In order to acquire information on the scattering dynamics, the laboratory data were transformed into the center-of-mass reference frame utilizing a forward-convolution routine.[76-78] This iterative method employs a parametrized or point-form angular flux distribution, $T(\theta)$, and translational energy flux distribution, $P(E_T)$, in the center-of-mass (CM) frame. Laboratory TOF spectra and the laboratory angular distributions are calculated from the $T(\theta)$ and $P(E_T)$ functions and are averaged over a grid of Newton diagrams accounting for the apparatus functions, beam divergences, and velocity spreads. During the analytical fitting, we considered an integral reactive scattering cross section with an $E_c^{-1/3}$ energy dependence with E_c being the collision energy. This energy dependence is exploited for barrier-less reactions dominated by long-range attractive forces within the line-of-center model.[79] The center-of-mass distributions can be combined as a flux contour map, $I(\theta,u) = P(u) \times T(\theta)$, which reports the flux of the reactively scattered products as a function of the center-of-mass scattering angle (θ) and product velocity (u). This plot acts as an image of the reaction and contains all the information of the scattering dynamics.[80]

Finally, we would like to highlight that only silylidyne radicals in the $^2\Pi$ ground electronic state participate in the reaction. The first electronic state $A^2\Delta$ that might be populated in photolysis process has a lifetime of only 534 ± 23 ns[81] and hence relaxes to the ground state before reaching the collision center. We further characterized the ro-vibrational energy distribution of the silylidyne radical in its ground electronic state ($X^2\Pi$) employing laser-induced fluorescence (LIF) for the $A^2\Delta \leftarrow X^2\Pi$ band.[82-84] Briefly, the beam of the detection laser propagated within the scattering plane and orthogonally intercepted the chopped section of the pulsed silylidyne radical beam. Fluorescence of electronically excited silylidyne via the $A^2\Delta \leftarrow$

$X^2\Pi$ transition around 412 nm was detected by a top-mounted photomultiplier tube Hamamatsu R955. Tunable radiation near 412 nm for $A^2\Delta \leftarrow X^2\Pi$ electronic excitation was produced by a Lambda Physik Scanmate dye laser with circulating Exalite 411 dye, pumped by the third harmonic of an integrated Nd:YAG laser operating at 10 Hz. We attenuated the 10 ns pulse energy to 10 μJ by reducing the apertures of irises in the beam path. An interference filter centered at 410 nm, with 10 nm FWHM transmission, was placed in front of the photomultiplier tube (PMT) to reduce ambient light exposure. The signal from PMT was pre-amplified in Hamamatsu C7247 socket assembly prior to a gated detection by a digital oscilloscope interfaced to a computer. In order to eliminate the observed baseline fluctuations due to electromagnetic interferences or pre-amplifier instability, we introduced a high pass filter between the pre-amplifier and the oscilloscope. The timing pulse sequence is compiled in Figure 3. The delay introduced by the first pulse/delay generator (PDG I) determines which part of the 80 μs pulse passes through the slit. PDG II controls the delay between the pulsed valve opening and the excimer laser photolysis pulse generation, and PDG III offsets the LIF pulse generation event by the time needed for the silylidyne radical beam traveling at 1730 ms^{-1} velocity to arrive in the interaction region. The resulting excitation LIF spectrum of silylidyne radicals in (0,0) $A^2\Delta \leftarrow X^2\Pi$ region is presented in Figure 4. The spectrum was analyzed utilizing a LIFBASE database and spectral simulation for diatomic molecules by Jorge Luque.[85] A single rotational temperature cannot reproduce the observed transitions. Best fits interpret the rotational state distribution as a sum of two thermalized distributions with 80 % of the silylidyne radicals at 40 ± 10 K and 20 % at 300 ± 50 K. The bimodal temperature distribution might be the result of two distinct formation pathways of silylidyne from disilane, which are well documented in the literature. Silylidyne radials can be formed via a single 193 nm photon absorption of disilane via reaction (3)[86] or through consecutive absorption of two photons (reactions (4) and (5)).[74] Therefore, the photo-dissociation of disilane produces apart from the silylidyne radical likely silane (SiH_4) as well as silyl radicals (SiH_3). We also conducted the search for the silyl radicals using TOF mass spectroscopy. No detectable levels of silyl radials were found. If these radicals are still in the beam at concentrations below our detection limit, silyl radicals were found to have very slow rate constants of only 10^{-14} cm^3 $molecule^{-1}$ s^{-1} upon reaction with unsaturated hydrocarbons.[87] Reactive scattering signal of silyl radicals with unsaturated hydrocarbons should not be observable under our experimental conditions. Note that we cannot resolve the degenerate spinorbit states of silylidyne radical, since the Λ-splitting for the SiH ground state $^2\Pi$ is 0.099 cm^{-1} that is lower than the resolution of the excitation dye laser (0.13 cm^{-1}).

(3) $Si_2H_6 + h\upsilon \rightarrow SiH_4 + SiH + H$

(4) $Si_2H_6 + h\upsilon \rightarrow 2\ SiH_3$

(5) $SiH_3 + h\upsilon \rightarrow SiH + H_2$

3. Theoretical Methods

Structures for the reactants, intermediates, and products were obtained via ωB97X-V/cc-pVTZ[88-89] geometry optimizations and frequency calculation. Transition state structures were computed using the freezing string method (FSM)[90-91] followed by a transition state search using the partitioned-rational function optimization (P-RFO) eigenvector-following method[92] and frequency calculation, also at the ωB97X-V/cc-pVTZ level. These vibrational frequency calculations confirm that the minima have no imaginary frequencies and the transition states have only one imaginary frequency. They additionally were used to calculate the harmonic zero-point energy corrections for all structures. All DFT calculations were carried out using an integration grid consisting of 99 radial points and 590 angular points. Except where otherwise specified, all energies are computed at the ωB97X-V/cc-pVTZ level. Energies of reactants, **p1,** and **p2** were additionally computed using coupled cluster with single, double, and perturbative triple excitations [CCSD(T)][93] utilizing a frozen core approximation and second-order Møller-Plesset perturbation theory.[94] To compare directly to experimental data, the reaction energies for **p1** and **p2** were computed via

$$\begin{aligned} E(CCSD(T)/CBS) \\ &= E(HF/cc-pV5Z) + E^{corr}(MP2/CBS_{4,5}) + E^{corr}(CCSD(T)/cc-pVTZ) \\ &- E^{corr}(MP2/cc-pVTZ) + ZPE(\omega B97X-V/cc-pVTZ) \end{aligned}$$

where $E^{corr}(MP2/CBS_{4,5})$ is the extrapolated MP2 correlation energy using the cc-pVQZ and cc-pV5Z basis sets and the extrapolation approach:[95]

$$\begin{aligned} E^{corr}\left(MP2/(CBS_{M,N})\right) \\ &= [N^3E^{corr}(MP2/cc-pVNZ) - M^3E^{corr}(MP2/cc-pVMZ)]/[N^3 - M^3] \end{aligned}$$

where M and N denote the cardinal number for the cc-pVNZ basis sets. These CCSD(T)/CBS energies are estimated to be converged to within 3 kJ mol^{-1}. Algorithms for calculating nucleus-independent chemical shift values were utilized to gauge the relative aromatic character of **p1** and similarly shaped comparable molecules.[96-97] These calculations were performed at the HF/cc-pVDZ and B3LYP/cc-pVDZ levels.[98-100] All calculations were performed using the QChem suite of electronic structure programs.[101] Please note that the coupled cluster results are a higher level benchmark that can be used to partially validate the density functional theory used to evaluate energies of the intermediates. In comparing the CCSD(T)/CBS reaction energies against the ωB97X-V/cc-pVTZ reaction energies, we see that the reaction energy is changed from -19.9 kJ mol^{-1} to -4.9 kJ mol^{-1}. This energy change is a measure of the uncertainty in the calculated relative energy of the intermediates.

4. Experimental Result

4.1. Laboratory Data

For the reaction of the silylidyne radical (SiH; 29 amu) with the allene molecule (C_3H_4; 40 amu), reactive scattering signal was observed at *m/z* = 68 ($SiC_3H_4^+$) (Figure 5). Signal at *m/z* = 67 ($SiC_3H_3^+$) was also recorded, but the corresponding time-of-flight spectra (TOF) depicted – after scaling – identical pattern as those obtained at *m/z* = 68 ($SiC_3H_4^+$). Therefore, we can conclude that signal at *m/z* = 67 actually originates from dissociative ionization of the parent molecule in the electron impact ionizer. Further, these results suggest that the silylidyne radical versus atomic hydrogen exchange pathways leading to a molecule with the molecular formula SiC_3H_4 is open and that the molecular hydrogen loss channel is closed under our experimental conditions. Finally, it is important to highlight that minor scattering signal was detected at *m/z* = 69, which is about 10% of that at *m/z* = 68. This implies the detection of the product $^{29}SiC_3H_4$ via an atomic hydrogen loss channel; further, no radiative association at *m/z* = 69 ($SiC_3H_5^+$) occurs in the current system; hence, the lifetime of the SiC_3H_5 adduct is too low to survive the flight time from the interaction region to the ionizer. We also searched for SiC_3H_6 isomers (*m/z* = 70) potentially formed via the reaction of silyl radicals (SiH_3; 31 amu) with allene (40 amu), but no signal was observed. This amplifies our previous conclusion that the concentration of silyl radicals is too low (or they are absent) to observe reactive scattering signal and/or that the rate constants and hence corresponding cross sections are lower by up to three orders of magnitude when compared to rate constants of silylidyne radical reactions with unsaturated hydrocarbons.

The TOF spectra at *m/z* = 68 ($SiC_3H_4^+$) were then recorded at distinct laboratory angles, integrated, and normalized with respect to the center-of-mass reference angle to obtain the laboratory product angular distribution (Figure 6). This distribution is relatively narrow and spans only about 25° within the scattering plane as defined by the primary and secondary beam. This suggests a relatively low translational energy release. The most probable Newton diagram for the reaction of the silylidyne radical (SiH; 29 amu) with the allene molecule (C_3H_4; 40 amu) leading to SiC_3H_4 (68 amu) plus atomic hydrogen (1 amu) is also displayed in Figure 6, contemplating the formation of the thermodynamically most stable SiC_3H_4 isomer 2-methyl-1-silacycloprop-2-enylidene (Figure 1).

Having provided evidence on the formation of SiC_3H_4 isomer(s) along with atomic hydrogen, we are attempting to probe to what extent the hydrogen atom originates from the allene molecule and/or from the silylidyne radical. For this, we conducted the reaction of the silylidyne radical (SiH; 29 amu) with D4-allene (C_3D_4; 44 amu). An atomic hydrogen loss should be reflected in scattering signal at *m/z* = 72 ($SiC_3D_4^+$), which can fragment to *m/z* = 70 ($SiC_3D_3^+$); on the other hand, an atomic deuterium loss is expected to lead to reactive scattering signal at *m/z* = 71 ($SiC_3D_3H^+$). This signal is unique to reactive scattering signal if the deuterium loss is open, but cannot arise from dissociative electron impact ionization of heavier reaction products. Considering that the reactive scattering signal was very weak along with economic limitations due to the costs of the D4-allene reactant, reactive scattering signal was probed only at the center-of-mass angle. As a result, signal was observed at *m/z* = 72 ($SiC_3D_4^+$, H-loss) *and* at *m/z* = 71 ($SiC_3D_3H^+$, D-loss) at a ratio of 1.0 to 1.5 (Figure 7). This finding indicates that both the atomic hydrogen and atomic deuterium loss channels are open and that the reaction mechanism involves at least two channels.

4.2. Center-of-Mass Functions

The CM translational energy distribution $P(E_T)$ is presented along with the center-of-mass angular distribution $T(\theta)$ in Figure 8. It is important to note that the experimental data could be nicely reproduced exploiting a single channel fit with the reactant masses of 29 amu (SiH) plus 40 amu (C_3H_4) and the product masses of 68 amu (SiC_3H_4) plus 1 amu (H). In detail, the $P(E_T)$ could be fit with a maximum translational energy release E_{max} of 50 ± 12 kJ mol^{-1}.

For products born without internal excitation, this high energy cutoff represents the sum of the collision energy plus the absolute value of the reaction exoergicity. A subtraction of the collision energy of 30.3 ± 0.7 kJ mol^{-1} from the maximum translational energy yields a reaction exoergicity of 19 ± 13 kJ mol^{-1}. Further, the $P(E_T)$ was found to peak at 10 ± 3 kJ mol^{-1}. This peaking relative close to zero translational energy indicates the existence of a relatively loose exit transition state upon formation of the SiC_3H_4 isomer(s) plus atomic hydrogen.[102] Finally, we computed the average fraction of the available energy channeling into the translational degrees of freedom to be 43 ± 11%.

We gain additional insights into the chemical dynamics of the reaction by inspecting the CM angular distribution $T(\theta)$. First, the $T(\theta)$ depicts flux over the complete angular range from 0° to 180° implying indirect scattering dynamics via complex formation along with the existence of bound SiC_3H_5 intermediate(s).[102] Secondly, $T(\theta)$ portrays a pronounced maximum at about 90°, suggesting that the atomic hydrogen emission occurs almost parallel to the total angular momentum vector **J** and nearly perpendicularly to the rotational plane of the decomposing intermediate(s).[80] Lastly, the $T(\theta)$ depicts a slight forward scattering with an intensity ratio $I(0^\circ)/ I(180^\circ)$ of about 1.25 ± 0.05. This finding proposes the existence of an osculating complex. Here, a complex formation takes place, but the well depth along the reaction coordinate is too shallow and/or the lifetime of the decomposing complex is too low to allow multiple rotations, such that the complex decomposes with a random lifetime distribution before one full rotation elapses.[103] We would like to stress that a forward-backward symmetric distribution leads to a slightly worse fits of the experimental data.

5. Discussion

In order to investigate the underlying reaction mechanisms of the silylidyne radical (SiH; 29 amu) with the allene molecule (C_3H_4; 40 amu), we are merging now the experimental results with the computational data. Let us compile the experimental results. *First*, the TOF spectra recorded at $m/z = 68$ depict evidence of the formation of product(s) with the molecular formula SiC_3H_4 (68 amu) along with atomic hydrogen (1 amu). Experiments of the silylidyne radical (SiH; 29 amu) with D4- allene (C_3D_4; 44 amu) provided further evidence via the detection of SiC_3D_4 (72 amu) *and* SiC_3D_3H (71 amu) together with atomic hydrogen and deuterium, respectively, that at least two (micro) channels exist. *Second*, the center-of-mass angular distribution $T(\theta)$ depicts that the reaction followed indirect scattering dynamics via SiC_3H_5 collision complex(es) holding lifetimes in the order of their rotational period. Further, the distribution maximum close to 90º suggests a preferential atomic hydrogen loss almost perpendicularly to the rotational plane of the decomposing complex(es). *Third*, the formation of SiC_3H_4 isomer(s) plus atomic hydrogen was found to be slightly exoergic by 19 ± 13 $kJmol^{-1}$; the exit transition state was found to be rather loose as reflected in the peaking of the $P(E_T)$ at only 10 ± 3 kJ mol^{-1}.

Having monitored the atomic hydrogen loss under single collision conditions, we are comparing first the experimentally derived reaction energy with the computed data to form distinct SiC_3H_4 product isomer(s). The electronic structure calculations reveal that only two SiC_3H_4 isomers are energetically accessible at our collision energy of 30.3 ± 0.7 kJ mol^{-1} (Figure 9). The structures of the reactants, intermediates, transition states, and products are also listed here (Table 1). We would like to stress that our computations revealed the existence of overall 28 product SiC_3H_4 isomers; the structures, energetics, and symmetries of the electronic ground states of these species are compiled in the Supplementary Material. Here, we are focusing on the computational data necessary to rationalize the experimental findings. The formation of the 2-methyl-1-silacycloprop-2-enylidene (**p1**) and silacyclobut-2-enylidene (**p2**) isomers was found to be exoergic (**p1**) and endoergic (**p2**) by 5 kJ mol^{-1} and 20 kJ mol^{-1}, respectively. The experimentally derived reaction energy of - 19 ± 13 $kJmol^{-1}$ correlates within the error limits nicely with the formation of the 2-methyl-1-silacycloprop-2-enylidene isomer (**p1**) and a computed exoergicity of 5 kJ mol^{-1}. Therefore, **p1** represents the major reaction product. However, we cannot exclude minor contribution of the thermodynamically less favorable product **p2** at a level of 12 ± 3 % assuming all product flux at translational energies of the products less than 10 $kJmol^{-1}$ contributes to **p2**.

We are now proposing the underlying reaction mechanism(s) by combining the experimental data with the electronic structure calculations. An examination of the molecular structures of the silylidyne and allene reactants together with the 2-methyl-1-silacycloprop-2-enylidene product (**p1**) suggests that the reaction involves multiple reaction steps. *First*, the hydrogen atom from the silylidyne radical must be either emitted and/or undergo hydrogen migration eventually to the C1 and/or C3 carbon atom of the allene moiety. *Second*, since the reaction of the silylidyne radical (SiH; 29 amu) with D4-allene (C_3D_4; 44 amu) provided evidence of the formation of

SiC_3D_4 (72 amu) *and* SiC_3D_3H (71 amu), a fraction of the hydrogen atoms from the silylidyne must be ejected to account for the detection of SiC_3D_4 (72 amu). *Third*, the emission of the deuterium atom must resemble a second reaction pathway to rationalize the synthesis of SiC_3D_3H (71 amu). *Fourth*, at least one hydrogen migration has to occur to the terminal $=CH_2$ moiety eventually forming a methyl group. *Finally*, the silylidyne radical is proposed to add either to one carbon atom (terminal, central) – followed by ring closure via addition to the central or terminal carbon atom – and/or to both carbon atoms of the allene reactant eventually forming a cyclic reaction intermediate.

The electronic structure calculations confirm these predictions and reveal that the silylidyne radical can react with the allene molecule via barrier-less addition to the terminal carbon atom (C1), the central carbon atom (C2), and simultaneously to the terminal and central carbon atom (C1-C2) leading to intermediates [i1], [i2], and [i3], respectively. These doublet collision complexes are stabilized by 37, 124, and 141 $kJmol^{-1}$ with respect to the reactants (Figure 9, Table 1). An insertion pathway of the silylidyne radical into the carbon-hydrogen bond of allene forming intermediate [i4] has an entrance barrier of 57 kJ mol^{-1} and is closed under our experimental conditions and a collision energy of 30 kJ mol^{-1}. These initial collision complexes can also isomerize to each other. Here, [i1] can undergo ring closure to [i3] via a barrier of only 5 kJ mol^{-1}. An alternative hydrogen shift from [i1] to [i4] is expected to be energetically less favorable considering an inherent barrier to hydrogen migration of 50 kJ mol^{-1}; further, this transition states ranges 13 kJ mol^{-1} above the separated reactants. Similar to [i1], [i2] rearranges via ring closure to [i3] through a barrier of only 34 kJ mol^{-1}.

Considering the geometries and connections of the atoms in these intermediates, none of the [i1] to [i4] structures, however, can decompose via atomic hydrogen loss to **p1**. Therefore, additional isomerization pathways of these intermediates – as predicted by the experimental data – must precede *any* unimolecular decomposition. As a matter of fact, our computations reveal the existence of six additional SiC_3H_4 isomers [i5] to [i10], which can be formed via hydrogen shifts and ring closures. The electronic structure calculations propose that intermediate [i1] can undergo a hydrogen shift from the C1 to the C2 carbon atom of the allene moiety leading to [i5]; however, the transition state is located 75 kJ mol^{-1} above the energy of the separated reactants. Considering the collision energy of about 30 $kJmol^{-1}$, this pathway is clearly closed under our experimental conditions. Further, intermediate [i2] can undergo hydrogen migration from the silicon atom to the terminal carbon atom of the allene moiety forming a methyl group of intermediate [i6]. This hydrogen shift is associated with a barrier of 60 kJ mol^{-1}, which lies well below the energy of the separated reactants. Intermediate [i3] was found to be connected to isomers [i7], [i8], and [i9]. The first isomerization from [i3] to [i7] involves a complex hydrogen migration – ring closure process, which is energetically not accessible in our experiments since the transition state lies 45 kJ mol^{-1} above the separated reactants. The [i3] to [i8] rearrangement proceeds via a hydrogen shift from the C1 to the C3 carbon atom via a barrier of 69 kJ mol^{-1}. The final pathway from [i3] follows also a hydrogen migration, but from the carbon atom to the SiH group forming [i9]. Considering that these pathways are associated with barriers ranging 186, 69, and 140 kJ mol^{-1} above [i3], the isomerization of [i3] should lead preferentially to [i8]. Finally, our computations reveal that intermediate [i4] can isomerizes to [i9] and [i10] via ring closure and hydrogen shift from the SiH_2 group to the terminal carbon atom involving barriers of 69 kJ mol^{-1} and 193 kJmol^{-1}, respectively. However, considering that [i4] cannot be preferentially accessed via insertion or isomerization of [i1] to [i3], the rearrangements of [i4] to [i9] and [i10] play very minor role in the reaction dynamics. Also, our calculations reveal five additional rearrangements of [i5] to [i10] among each other. Both rearrangement from [i7] to [i8] via a hydrogen migration – ring opening – ring closure and [i9] to [i8] through hydrogen migration hold transition state well above the experimental collision energy (138 kJ mol^{-1} and 91 kJ mol^{-1}) and hence cannot be accessed. Although an energetically accessible transition state connects [i5] to [i7] via ring closure, this pathway is irrelevant to the reaction mechanisms, since isomer [i5] was found not to be accessible at a collision energy of 30 kJ mol^{-1}. Likewise, the ring closure from [i10] to [i8] plays no role, since we concluded that [i10] cannot be accessed either. However, the simultaneous hydrogen shift from the CH_2 moiety and ring closure from [i6] to [i8] is associated with a barrier ranging 61 kJ mol^{-1} below the separated reactants. Finally, intermediate [i8] can be classified as the decomposing complex forming the product **p1** via atomic hydrogen loss from the silicon atom via a loose exit transition state.

We would like now to propose the underlying reaction mechanism(s). The computations suggest that the silylidyne radical adds barrierlessly via three feasible entrance channels to form intermediates [i1] to [i3] (Figure 9). This indirect reaction dynamics via complex formation were inferred experimentally from the center-of-mass angular distribution depicting intensity over the whole scattering range (Figure 8). Considering that intermediates [i1] and [i2] can undergo ring closure to [i3] with barriers less than the energy of the separate reactants, four pathways do exist which lead eventually to the decomposing complex [i8]: [i1]/[i2] →[i3] → [i8] (pathway 1), [i2] → [i6] → [i8] (pathway 2), ([i1]/[i2] →)[i3] → [i7] → [i8] (pathway 3) and ([i1]/[i2] →)[i3] → [i9] → [i8] (pathway 4). Considering the inherent barriers to isomerization as discussed above, pathways 1 (Figure 9, blue pathway) and 2 (Figure 9, red pathway) should be favorable compared to pathways 3 and 4. Eventually, intermediate [i8] undergoes unimolecular decomposition via atomic hydrogen loss from the silylidyne moiety forming the product **p1**. Our electronic structure calculations predict a barrierless dissociation; the experimental analysis indicates this process is associated with a rather loose transition state based on the weakly off-zero peaking of the center of mass translational energy distribution at only about 10 ± 3 kJ mol^{-1}. Considering the reversed reaction, i.e. the addition of the hydrogen atom to the closed shell product **p1**, the potential existence of a small entrance barrier to hydrogen atom addition might be reasonable, in particular since **p1** is partially aromatic (2 π) holding a nucleus-independent chemical shift (NICS) value of -17.6. Compared to the NICS value of silacyclopropenylidene (c-SiC_2H_2) of -15.7, **p1** demonstrates slightly more aromatic character (Table 3).

Finally, we would like to integrate the experimental finding of an atomic hydrogen and deuterium loss in the silylidyne – D4-allene system and see if the proposed reaction pathways (1) and (2) are consistent with the experimental data of a hydrogen loss and a deuterium loss. Figure 10 visualizes both reaction pathways by distinguishing hydrogen and deuterium atoms. Here, in all initial collision complexes [i1’] to [i3’], the hydrogen atom is connected to the silicon atom. Considering pathway 1, which involves the sequence ([i1’]/[i2’] →)[i3’] → [i8’], the hydrogen atoms is always connected to the silicon atom, since only one deuterium atom is involved in the hydrogen migration from the C1 carbon atom to the C3 carbon atom of the D4-allene moiety, resulting into the formation a CD_3 group in the C3 carbon atom and a double bond between C1 and C2 carbon atoms. In pathway 2 ([i2’] → [i6’] → [i8’]), however, a hydrogen atom will migrate from the silicon atom to the terminal carbon atom to from a CD_2H group in the C3 carbon atom of the D4-allene moiety, followed by a deuterium atom migration from the C1 carbon atom to the silicon atom as well as the cyclization between the silicon and C1-C2 atoms to yield [i8”], i.e. an isotopologue of [i8’]. Therefore, in the silylidyne – D4-allene system, two distinct intermediates exist ([i8’] and [i8”]), which can decompose via an atomic hydrogen loss (pathway 1) from [i8'] *and* also via an atomic deuterium loss (pathway 2) from [i8"]. Recall that signal was observed at *m/z* = 72 ($SiC_3D_4^+$) and at *m/z* = 71 ($SiC_3D_3H^+$) at a ratio of 1.0 to 1.5. However, we have to keep in mind that the reactants carry one hydrogen atom, but four deuterium atoms. Therefore, the experimentally determined ratio of the signal of the hydrogen versus deuterium loss channel of 1.0 : 1.5 changes to 2.7 : 1.0, if we account for the statistical factor and the availability of deuterium versus hydrogen in the reactants, i.e. preference of the hydrogen atom loss channel (pathway 1) compared to the deuterium loss channel (pathway 2). Therefore, at least two mechanisms exist to form c-SiC_3H_4 (**p1**) and hence c-SiC_3D_4 and c-SiC_3D_3H under single collision conditions.

6. Summary

We conducted the crossed molecular beam reaction of the ground state silylidyne radical (SiH; $X^2\Pi$) with allene (H_2CCCH_2; X^1A_1) and with D4-allene (D_2CCCD_2; X^1A_1) at collision energies of about 30 kJ mol^{-1}. Electronic structure calculations propose that the reaction of silylidyne with allene has no barrier and is initiated by silylidyne radical addition to the π electron density of the allene molecule either to one carbon atom (C1 and/or C2) or to both carbon atoms simultaneously. These indirect (complex forming) scattering dynamics were also confirmed by the center-of-mass angular distribution. The initially formed addition complexes [i1] to [i3] were found to isomerize via two reaction pathways leading both eventually to the cyclic SiC_3H_4 intermediate [i8]. The latter decomposed via atomic hydrogen loss through a loose exit transition state located only 3 kJ mol^{-1} above the energy of the separated reactants via atomic hydrogen loss perpendicularly to the plane of the decomposing complex (sideways scattering) in an overall exoergic reaction (experimentally: - 19 ± 13 kJ mol^{-1}; computationally: - 5 kJ ± 3 kJ mol^{-1}). The silylidyne with D4-allene system elucidated the details of the reaction pathways by an identification of both the atomic hydrogen and deuterium loss pathways leading to SiC_3D_4 and SiC_3HD_3 isomers, respectively, under single collision conditions. Here, the first reaction pathway proceeded via intermediate [i3] formed either from the reactants via cyclization of [i1] and/or [i2]; the latter undergoes hydrogen shift to form eventually [i8]. The second channel involves a hydrogen migration from [i2] to [i6], which then undergoes yet another hydrogen shift to [i8]. Note that for both channels, the four heavy atoms are rotating in the plane almost perpendicular to the total angular momentum vector **J**. Considering the microcanonical model of Grice and

Smith,[104] such a hydrogen loss leads to a preferential hydrogen elimination almost parallel to the total angular momentum vector, and the resulting peaked center-of-mass angular distribution as observed experimentally and predicted computationally. This hydrogen loss yields eventually to the hitherto elusive and aromatic 2-methyl-1-sila-cycloprop-2-enylidene molecule (SiC_3H_4), which can be derived from the closed shell cyclopropenylidene molecule ($c\text{-}C_3H_2$) by replacing a hydrogen atom by a methyl group, and the carbene carbon atom by an isovalent silicon. The formation of the 2-methyl-1-silacycloprop-2-enylidene molecule in the bimolecular gas reaction of silylidyne with allene enriches our understanding toward the formation of organosilicon species in the interstellar medium gas phase – in particular of barrier-less, exoergic reactions, thus opening up a versatile approach to form hitherto poorly characterized silicon-bearing species in extraterrestrial environments.

Acknowledgements

T. Yang, B. B. Dangi, P. Maksyutenko, and R. I. Kaiser thank the National Science Foundation (NSF) for support under award CHE-1360658.

References

1. Kwok, S. *Organic Matter in the Universe*; John Wiley & Sons: **2011**.
2. Millar, T.; Herbst, E.; Bettens, R. Large Molecules in the Envelope Surrounding IRC+10216. *Mon. Not. R. Astron. Soc.* **2000,** *316*, 195-203.
3. Ziurys, L. M. The Chemistry in Circumstellar Envelopes of Evolved Stars: Following the Origin of the Elements to the Origin of Life. *Proc. Natl. Acad. Sci. U.S.A.* **2006,** *103*, 12274-12279.
4. Agúndez, M.; Cernicharo, J.; Pardo, J.; Expósito, J. F.; Guélin, M.; Tenenbaum, E.; Ziurys, L.; Apponi, A. Understanding the Chemical Complexity in Circumstellar Envelopes of C-Rich AGB stars: the Case of IRC+ 10216. *Astrophys. Space Sci.* **2008,** *313*, 229-233.
5. Van Orden, A.; Giesen, T.; Provencal, R.; Hwang, H.; Saykally, R. Characterization of Silicon–carbon Clusters by Infrared Laser Spectroscopy: The ν3 (σu) Band of Linear Si_2C_3. *J. Chem. Phys.* **1994,** *101*, 10237-10241.
6. Van Orden, A.; Provencal, R.; Giesen, T.; Saykally, R. Characterization of Silicon-carbon Clusters by Infrared Laser Spectroscopy. The ν1 Band of SiC_4. *Chem. Phys. Lett.* **1995,** *237*, 77-80.
7. Kokkin, D.; Brünken, S.; Young, K.; Patel, N.; Gottlieb, C.; Thaddeus, P.; McCarthy, M. The Rotational Spectra of $^{29}SiC_2$ and $^{30}SiC_2$. *Astrophys. J. Suppl. S.* **2011,** *196*, 17.
8. Stanton, J. F.; Dudek, J.; Theulé, P.; Gupta, H.; McCarthy, M.; Thaddeus, P. Laser Spectroscopy of Si_3C. *J. Chem. Phys.* **2005,** *122*, 124314-124314.
9. Guélin, M.; Muller, S.; Cernicharo, J.; Apponi, A.; McCarthy, M.; Gottlieb, C.; Thaddeus, P. Astronomical Detection of the Free Radical SiCN. *Astron. Astrophys.* **2000,** *363*, L9-L12.
10. McCarthy, M.; Gottlieb, C.; Thaddeus, P. Silicon Molecules in Space and in the Laboratory. *Mol. Phys.* **2003,** *101*, 697-704.
11. Apponi, A.; McCarthy, M.; Gottlieb, C.; Thaddeus, P. The Radio Spectra of SiCCH, SiCN, and SiNC. *Astrophys. J. Lett.* **2000,** *536*, L55.
12. Kaiser, R.; Stranges, D.; Lee, Y.; Suits, A. Neutral-neutral Reactions in the Interstellar Medium. I. Formation of Carbon Hydride Radicals via Reaction of Carbon Atoms with Unsaturated Hydrocarbons. *Astrophys. J.* **1997,** *477*, 982.
13. Kaiser, R. I.; Balucani, N.; Charkin, D. O.; Mebel, A. M. A Crossed Beam and ab initio Study of the $C_2(X^1\Sigma_g^+/a^3\Pi_u) + C_2H_2(X^1\Sigma_g^+)$ Reactions. *Chem. Phys. Lett.* **2003,** *382*, 112-119.
14. Kaiser, R.; Chiong, C.; Asvany, O.; Lee, Y.; Stahl, F.; Schleyer, P. v. R.; Schaefer III, H. Chemical Dynamics of D1-methyldiacetylene (CH_3CCCCD; X^1A_1) and D1-ethynylallene ($H_2CCCH(C_2D)$; X^1A') Formation from Reaction of C_2D ($X^2\Sigma^+$) with Methylacetylene, CH_3CCH (X^1A_1). *J. Chem. Phys.* **2001,** *114*, 3488-3496.
15. Ziurys, L. M. The Chemistry in Circumstellar Envelopes of Evolved Stars: Following the Origin of the Elements to the Origin of Life. *Proc. Natl. Acad. Sci. U.S.A.* **2006,** *103*, 12274-12279.
16. MacKay, D.; Charnley, S. The Silicon Chemistry of IRC+ 10° 216. *Mon. Not. R. Astron. Soc.* **1999,** *302*, 793-800.
17. Marvel, K. B. No Methane Here. The HCN Puzzle: Searching for CH_3OH and C_2H in Oxygen-rich Stars. *Astron. J.* **2005,** *130*, 261.
18. Charnley, S.; Ehrenfreund, P.; Kuan, Y.-J. Spectroscopic Diagnostics of Organic Chemistry in the Protostellar Environment. *Spectrochim. Acta A: Mol. Biomol. Spectrosc.* **2001,** *57*, 685-704.
19. Woodall, J.; Agúndez, M.; Markwick-Kemper, A.; Millar, T. The UMIST Database for Asrochemistry 2006. *Astron. Astrophys.* **2007,** *466*, 1197-1204.
20. Wakelam, V.; Herbst, E.; Loison, J.-C.; Smith, I.; Chandrasekaran, V.; Pavone, B.; Adams, N.; Bacchus-Montabonel, M.-C.; Bergeat, A.; Béroff, K. A Kinetic Database for Astrochemistry (KIDA). *Astrophys. J. Suppl. S.* **2012,** *199*, 21.
21. Morata, O.; Herbst, E. Time-dependent Models of Dense PDRs with Complex Molecules. *Mon. Not. R. Astron. Soc.* **2008,** *390*, 1549-1561.

22. Lis, D. C.; Blake, G. A.; Herbst, E. In *Astrochemistry: Recent Successes and Current Challenges*, Astrochemistry: Recent Successes and Current Challenges, 2005.

23. Wakelam, V.; Smith, I.; Herbst, E.; Troe, J.; Geppert, W.; Linnartz, H.; Öberg, K.; Roueff, E.; Agúndez, M.; Pernot, P. Reaction Networks for Interstellar Chemical Modelling: Improvements and Challenges. *Space Sci. Rev.* **2010,** *156*, 13-72.

24. Yasuda, Y.; Kozasa, T. Formation of SiC Grains in Pulsation-enhanced Dust-driven Wind around Carbon-rich Asymptotic Giant Branch Stars. *Astrophys. J.* **2012,** *745*, 159.

25. Willacy, K.; Cherchneff, I. Silicon and Sulphur Chemistry in the Inner Wind of IRC+ 10216. *Astron. Astrophys.* **1998,** *330*, 676-684.

26. Bettens, R.; Lee, H.-H.; Herbst, E. The Importance of Classes of Neutral-neutral Reactions in the Production of Complex Interstellar Molecules. *Astrophys. J.* **1995,** *443*, 664-674.

27. Millar, T.; Herbst, E. A New Chemical Model of the Circumstellar Envelope Surrounding IRC+ 10216. *Astron. Astrophys.* **1994,** *288*, 561-571.

28. Tenenbaum, E.; Dodd, J.; Milam, S.; Woolf, N.; Ziurys, L. The Arizona Radio Observatory 1 mm Spectral Survey of IRC+ 10216 and VY Canis Majoris (215–285 GHz). *Astrophys. J. Suppl. S.* **2010,** *190*, 348.

29. Tenenbaum, E.; Dodd, J.; Milam, S.; Woolf, N.; Ziurys, L. Comparative Spectra of Oxygen-rich Versus Carbon-rich Circumstellar Shells: VY Canis Majoris and IRC+ 10216 at 215-285 GHz. *Astrophys. J. Lett.* **2010,** *720*, L102.

30. Ziurys, L.; Halfen, D.; Woolf, N. In *Establishing the Synthetic Contingencies for Life: Following the Carbon from AGB Stars to Planetary Surfaces*, Bioastronomy 2007: Molecules, Microbes and Extraterrestrial Life, 2009; 59.

31. Woodall, J.; Agúndez, M.; Markwick-Kemper, A.; Millar, T. The UMIST Database for Astrochemistry 2006. *Astron. Astrophys.* **2007,** *466*, 1197-1204.

32. McElroy, D.; Walsh, C.; Markwick, A.; Cordiner, M.; Smith, K.; Millar, T. The UMIST Database for Astrochemistry 2012. *Astron. Astrophys.* **2013,** *550*, A36.

33. Millar, T. Silicon Chemistry in Dense Clouds. *Astrophys. Space Sci.* **1980,** *72*, 509-517.

34. Brown, J.; Millar, T. Modelling Enhanced Density Shells in the Circumstellar Envelope of IRC+ 10216. *Mon. Not. R. Astron. Soc.* **2003,** *339*, 1041-1047.

35. Howe, D.; Millar, T. The Formation of Carbon Chain Molecules in IRC+ 10216. *Mon. Not. R. Astron. Soc.* **1990,** *244*, 444-449.

36. Gensheimer, P.; Likkel, L.; Snyder, L. Full synthesis maps of circumstellar SiC2 in IRC+ 10216. *Astrophys. J.* **1995,** *439*, 445-454.

37. Kaiser, R.; Gu, X. Chemical Dynamics of the Formation of the Ethynylsilylidyne Radical (SiCCH (X^2P)) in the Crossed Beam Reaction of Ground State Silicon Atoms (Si(^3P)) with Acetylene (C_2H_2 ($X^1\Sigma_g^+$)). *J. Chem. Phys.* **2009,** *131*, 104311.

38. Parker, D. S.; Wilson, A. V.; Kaiser, R. I.; Mayhall, N. J.; Head-Gordon, M.; Tielens, A. G. On the Formation of Silacyclopropenylidene (c-SiC_2H_2) and its Role in the Organosilicon Chemistry in the Interstellar Medium. *Astrophys. J.* **2013,** *770*, 33.

39. Sattelmeyer, K. W.; Schaefer III, H. F.; Stanton, J. F. The Global Minimum Structure of SiC_3: the Controversy Continues. *J. Chem. Phys.* **2002,** *116*, 9151-9153.

40. Stanton, J. F.; Gauss, J.; Christiansen, O. Equilibrium Geometries of Cyclic SiC_3 Isomers. *J. Chem. Phys.* **2001,** *114*, 2993-2995.

41. Kenny, J. P.; Allen, W. D.; Schaefer, H. F. Complete basis set Limit Studies of Conventional and R12 Correlation Methods: the Silicon Dicarbide (SiC_2) Barrier to Linearity. *J. Chem. Phys.* **2003,** *118*, 7353-7365.

42. Sari, L.; Gonzales, J. M.; Yamaguchi, Y.; Schaefer III, H. F. The $\tilde{X}^2\Pi$ and $\tilde{A}^2\Sigma^+$ Electronic States of the HCSi Radical: Characterization of the Renner–Teller Effect in the Ground State. *J. Chem. Phys.* **2001,** *114*, 4472-4478.

43. Wang, H. J.; Schleyer, P. v. R.; Wu, J. I.; Wang, Y.; Wang, H. J. A Study of Aomatic Three Membered Rings. *Int. J. Quant. Chem.* **2011,** *111*, 1031-1038.

44. von Schleyer, P. R., The Contrasting Strain Energies of Small Ring Carbon and Silicon Rings. The Relationship with free Radical Energies. In *Substituent Effects in Radical Chemistry*, Springer: 1986; pp 69-81.

45. Sander, W.; Trommer, M.; Patyk, A. Oxidation of Silenes and Silylenes: Matrix Isolation of Unusual Silicon Species. *Organosilicon Chemistry Set: From Molecules to Materials* **2008**, 86-94.

46. von Ragué Schleyer, P.; Jiao, H.; Goldfuss, B.; Freeman, P. K. Aromaticity and Antiaromaticity in Five‐Membered C4H4X Ring Systems: “Classical” and “Magnetic” Concepts May Not Be “Orthogonal”. *Angew. Chem. Int. Edit.* **1995,** *34*, 337-340.

47. Schleyer, P. v. R.; Kost, D. A Comparison of the Energies of Double Bonds of Second-row Elements with Carbon and Silicon. *J. Am. Chem. Soc.* **1988,** *110*, 2105-2109.

48. Fernández, I.; Duvall, M.; Schleyer, P. v. R.; Frenking, G. Aromaticity in Group 14 Homologues of the Cyclopropenylium Cation. *Chem.--Eur. J.* **2011,** *17*, 2215-2224.

49. Thomas, P. S.; Bowling, N. P.; Burrmann, N. J.; McMahon, R. J. Dialkynyl Carbene Derivatives: Generation and Characterization of Triplet *tert*-Butylpentadiynylidene (*t*-Bu-C≡C-C$^{\cdot}$-C≡C-H) and Dimethylpentadiynylidene (Me-C≡C-C$^{\cdot}$-C≡C-Me). *J. Org. Chem.* **2010,** *75*, 6372-6381.

50. Seburg, R. A.; Patterson, E. V.; McMahon, R. J. Structure of Triplet Propynylidene (HCCCH) as Probed by IR, UV/vis, and EPR Spectroscopy of Isotopomers. *J. Am. Chem. Soc.* **2009,** *131*, 9442-9455.

51. Thomas, P. S.; Bowling, N. P.; McMahon, R. J. Spectroscopy and Photochemistry of Triplet Methylpentadiynylidene (Me-C≡C-C$^{\cdot}$-C≡C-H). *J. Am. Chem. Soc.* **2009,** *131*, 8649-8659.

52. Huang, L.; Asvany, O.; Chang, A.; Balucani, N.; Lin, S.; Lee, Y.; Kaiser, R.; Osamura, Y. Crossed Beam Reaction of Cyano Radicals with Hydrocarbon Molecules. IV. Chemical Dynamics of Cyanoacetylene (HCCCN; $X^1\Sigma^+$) Formation from Reaction of CN ($X^2\Sigma^+$) with Acetylene, C_2H_2 ($X^1\Sigma_g^+$). *J. Chem. Phys.* **2000,** *113*, 8656-8666.

53. Balucani, N.; Asvany, O.; Chang, A.; Lin, S.; Lee, Y.; Kaiser, R.; Osamura, Y. Crossed Beam Reaction of Cyano Radicals with Hydrocarbon Molecules. III. Chemical Dynamics of Vinylcyanide (C_2H_3CN; X^1A') Formation from Reaction of CN($X^2\Sigma^+$) with Ethylene, C_2H_4(X^1A_g). *J. Chem. Phys.* **2000,** *113*, 8643-8655.

54. Huang, L.; Lee, Y.; Kaiser, R. Crossed Beam Reaction of the Cyanogen Radical, CN ($X^2\Sigma^+$), with Acetylene, C_2H_2 ($X^1\Sigma_g^+$): Observation of Cyanoacetylene, HCCCN ($X^1\Sigma^+$). *J. Chem. Phys.* **1999,** *110*, 7119-7122.

55. Parker, D.; Mebel, A.; Kaiser, R. The Role of Isovalency in the Reactions of the Cyano (CN), Boron Monoxide (BO), Silicon Nitride (SiN), and Ethynyl (C_2H) Radicals with Unsaturated Hydrocarbons Acetylene (C_2H_2) and Ethylene (C_2H_4). *Chem. Soc. Rev.* **2014,** *43*, 2701-2713.

56. Parker, D. S.; Wilson, A. V.; Kaiser, R. I.; Labrador, T.; Mebel, A. M. Synthesis of the Silaisocyanoacetylene Molecule. *J. Am. Chem. Soc.* **2012,** *134*, 13896-13901.

57. Parker, D.; Wilson, A.; Kaiser, R.; Labrador, T.; Mebel, A. Gas-Phase Synthesis of the Silaisocyanoethylene Molecule (C_2H_3NSi). *J. Org. Chem.* **2012,** *77*, 8574-8580.

58. Chapman, O.; Chang, C.; Kolc, J.; Jung, M.; Lowe, J.; Barton, T. J.; Tumey, M. 1, 1, 2-Trimethylsilaethylene. *J. Am. Chem. Soc.* **1976,** *98*, 7844-7846.

59. Schriver, G. W.; Fink, M. J.; Gordon, M. S. Ab initio Calculations on Some C_3SiH_4 Isomers. *Organometallics* **1987,** *6*, 1977-1984.

60. Gordon, M. S. Ab initio Study of the Stabilities of Silacyclobutadiene and Silatetrahedrane (Silatricyclo [1.1.0.0^{2,4}]butane). *J. Chem. Soc., Chem. Comm.* **1980**, 1131-1132.

61. Maier, G.; Reisenauer, H. P.; Meudt, A. Silylenes of the Elemental Composition C_4H_2Si: Generation and Matrix‐Spectroscopic Identification. *Eur.J. Org. Chem.* **1998,** *1998*, 1285-1290.

62. Veszprémi, T.; Takahashi, M.; Ogasawara, J.; Sakamoto, K.; Kira, M. An ab initio MO Study of Structure and Reactivity of 4-silatriafulvene. *J. Am. Chem. Soc.* **1998,** *120*, 2408-2414.

63. Bachrach, S. M.; Liu, M. Structure, Topological Electron Density Analysis and Aromaticity of 4-heterosubstituted Methylenecyclopropenes: X=X=CH_2, NH, O, SiH_2, PH and S. *J. Phys. Org. Chem.* **1991,** *4*, 242-250.

64. Sakamoto, K.; Ogasawara, J.; Sakurai, H.; Kira, M. The First Silatriafulvene Derivative: Generation, Unusually Low Reactivity toward Alcohols, and Isomerization to Silacyclobutadiene. *J. Am. Chem. Soc.* **1997,** *119*, 3405-3406.

65. Sakamoto, K.; Ogasawara, J.; Kon, Y.; Sunagawa, T.; Kabuto, C.; Kira, M. The First Isolable 4-Silatriafulvene. *Angew. Chem. Int. Edit.* **2002,** *114*, 1460-1462.

66. Gentle, T. M.; Muetterties, E. Silane Surface Chemistry of Palladium: Synthesis of Silaethylene, Silacyclobutadiene and Silabenzene. *J. Am. Chem. Soc.* **1983,** *105*, 304-305.

67. Fink, M. J.; Puranik, D. B.; Johnson, M. P. Silacyclobutadienes: Generation of 1-mesityl-2,3,4-tri-tert-butyl-1-silacyclobutadiene. *J. Am. Chem. Soc.* **1988,** *110*, 1315-1316.

68. Puranik, D. B. Ph.D. thesis, The Synthesis and Chemistry of Silacyclobutadienes. Tulane University 1989.

69. Gu, X.; Kaiser, R. I. Reaction Dynamics of Phenyl Radicals in Extreme Environments: A Crossed Molecular Beam Study. *Acc. Chem. Res.* **2008,** *42*, 290-302.

70. Guo, Y.; Gu, X.; Kawamura, E.; Kaiser, R. I. Design of a Modular and Versatile Interlock System for Ultrahigh Vacuum Machines: A Crossed Molecular Beam Setup as a Case Study. *Rev. Sci. Instrum.* **2006,** *77*, 034701.

71. Gu, X.; Guo, Y.; Zhang, F.; Mebel, A. M.; Kaiser, R. I. Reaction Dynamics of Carbon-bearing Radicals in Circumstellar Envelopes of Carbon Stars. *Faraday Discuss.* **2006,** *133*, 245-275.

72. Kaiser, R. I.; Maksyutenko, P.; Ennis, C.; Zhang, F.; Gu, X.; Krishtal, S. P.; Mebel, A. M.; Kostko, O.; Ahmed, M. Untangling the Chemical Evolution of Titan's Atmosphere and Surface–from Homogeneous to Heterogeneous Chemistry. *Faraday Discuss.* **2010,** *147*, 429-478.

73. Zhang, F.; Kim, S.; Kaiser, R. I. A Crossed Molecular Beams Study of the Reaction of the Ethynyl Radical ($C_2H(X^2\Sigma^+)$) with Allene (H_2CCCH_2 (X^1A_1)). *Phys. Chem. Chem. Phys.* **2009,** *11*, 4707-4714.

74. Muranaka, Y.; Motooka, T.; Lubben, D.; Greene, J. Ultraviolet-laser Photolysis of Disilane. *J. Appl. Phys.* **1989,** *66*, 910-914.

75. Engelking, P. C. Spectroscopy of Jet-cooled Ions and Radicals. *Chem. Rev.* **1991,** *91*, 399-414.

76. Veron, M. Ph. D. thesis, University of California at Berkeley, Berkeley, California, 1981.

77. Weiss, M. S. Ph. D. thesis, University of California at Berkeley, Berkeley, California, 1986.

78. Kaiser, R. I.; Le, T. N.; Nguyen, T. L.; Mebel, A. M.; Balucani, N.; Lee, Y. T.; Stahl, F.; Schleyer, P. v. R.; Schaefer Iii, H. F. A Combined Crossed Molecular Beam and ab initio Investigation of C_2 and C_3 Elementary Reactions with Unsaturated Hydrocarbons—Pathways to Hydrogen Deficient Hydrocarbon Radicals in Combustion Flames. *Faraday Discuss.* **2002,** *119*, 51-66.

79. Levine, R. D.; Bernstein, R. B.; Lee, Y. T. Molecular Reaction Dynamics and Chemical Reactivity. *Phys. Today* **1988**, 90.

80. Kaiser, R.; Parker, D.; Zhang, F.; Landera, A.; Kislov, V.; Mebel, A. PAH Formation under Single Collision Conditions: Reaction of Phenyl Radical and 1, 3-Butadiene to Form 1, 4-Dihydronaphthalene. *J. Phys. Chem. A* **2012,** *116*, 4248-4258.

81. Bauer, W.; Becker, K. H.; Düren, R.; Hubrich, C.; Meuser, R. Radiative Lifetime Measurements of SiH ($A^2\Delta$) by Laser-induced Fluorescence. *Chem. Phys. Lett.* **1984,** *108*, 560-561.

82. Nemoto, M.; Suzuki, A.; Nakamura, H.; Shibuya, K.; Obi, K. Electronic Quenching and Chemical Reactions of SiH Radicals in the Gas Phase. *Chem. Phys. Lett.* **1989,** *162*, 467-471.

83. Nozaki, Y.; Kongo, K.; Miyazaki, T.; Kitazoe, M.; Horii, K.; Umemoto, H.; Masuda, A.; Matsumura, H. Identification of Si and SiH in Catalytic Chemical Vapor Deposition of SiH_4 by Laser Induced Fluorescence Spectroscopy. *J. Appl. Phys.* **2000,** *88*, 5437-5443.

84. Maksyutenko, P.; Parker, D. S.; Zhang, F.; Kaiser, R. I. An LIF Characterization of Supersonic BO($X^2\Sigma^+$) and CN ($X^2\Sigma^+$) Radical Sources for Crossed Beam Studies. *Rev. Sci. Instrum.* **2011,** *82*, 083107.

85. Luque, J.; Crosley, D. R. LIFBASE: Database and Spectral Simulation Program (Version 1.5) **1999**.

86. Tada, N.; Tonokura, K.; Matsumoto, K.; Koshi, M.; Miyoshi, A.; Matsui, H. Photolysis of Disilane at 193 nm. *J. Phys. Chem. A* **1999,** *103*, 322-329.

87. Loh, S.; Jasinski, J. Direct Kinetic Studies of SiH_3+SiH_3, H, CCl_4, SiD_4, Si_2H_6, and C_3H_6 by Tunable Infrared Diode Laser Spectroscopy. *J. Chem. Phys.* **1991,** *95*, 4914-4926.

88. Mardirossian, N.; Head-Gordon, M. ωB97X-V: A 10-Parameter, Range-separated Hybrid, Generalized Gradient Approximation Density Functional with Nonlocal Correlation, Designed by a Survival-of-the-fittest Strategy. *Phys. Chem. Chem. Phys.* **2014,** *16*, 9904-9924.

89. Kendall, R. A.; Dunning Jr, T. H.; Harrison, R. J. Electron Affinities of the First-row Atoms Revisited. Systematic Basis Sets and Wave Functions. *J. Chem. Phys.* **1992,** *96*, 6796-6806.

90. Behn, A.; Zimmerman, P. M.; Bell, A. T.; Head-Gordon, M. Efficient Exploration of Reaction Paths via a Freezing String Method. *J. Chem. Phys.* **2011,** *135*, 224108.

91. Mallikarjun Sharada, S.; Zimmerman, P. M.; Bell, A. T.; Head-Gordon, M. Automated Transition State Searches without Evaluating the Hessian. *J. Chem. Theo. Comp.* **2012,** *8*, 5166-5174.

92. Baker, J. An Algorithm for the Location of Transition States. *J. Comp. Chem.* **1986,** *7*, 385-395.

93. Raghavachari, K.; Trucks, G. W.; Pople, J. A.; Head-Gordon, M. A Fifth-order Perturbation Comparison of Electron Correlation Theories. *Chem. Phys. Lett.* **1989,** *157*, 479-483.

94. Møller, C.; Plesset, M. S. Note on an Approximation Treatment for Many-electron Systems. *Phys. Rev.* **1934,** *46*, 618.

95. Halkier, A.; Helgaker, T.; Jørgensen, P.; Klopper, W.; Koch, H.; Olsen, J.; Wilson, A. K. Basis-set Convergence in Correlated Calculations on Ne, N_2, and H_2O. *Chem. Phys. Lett.* **1998,** *286*, 243-252.

96. Ochsenfeld, C.; Kussmann, J.; Koziol, F. Ab Initio NMR Spectra for Molecular Systems with a Thousand and More Atoms: A Linear‐Scaling Method. *Angew. Chem. Int. Edit.* **2004,** *43*, 4485-4489.

97. Kussmann, J.; Ochsenfeld, C. Linear-scaling Method for Calculating Nuclear Magnetic Resonance Chemical Shifts using Gauge-including Atomic Orbitals within Hartree-Fock and Density-functional Theory. *J. Chem. Phys.* **2007,** *127*, 054103.

98. Becke, A. D. Density-functional Exchange-energy Approximation with Correct Asymptotic Behavior. *Phys. Rev. A* **1988,** *38*, 3098.

99. Becke, A. D. Density-functional Thermochemistry. III. The Role of Exact Exchange. *J. Chem. Phys.* **1993,** *98*, 5648-5652.

100. Stephens, P.; Devlin, F.; Chabalowski, C.; Frisch, M. J. Ab initio Calculation of Vibrational Absorption and Circular Dichroism Spectra using Density Functional Force Fields. *J. Phys. Chem.* **1994,** *98*, 11623-11627.

101. Shao, Y.; Gan, Z.; Epifanovsky, E.; Gilbert, A. T.; Wormit, M.; Kussmann, J.; Lange, A. W.; Behn, A.; Deng, J.; Feng, X. Advances in Molecular Quantum Chemistry Contained in the Q-Chem 4 Program Package. *Mol. Phys.* **2015,** *113*, 184-215.

102. Levine, R. D. *Molecular Reaction Dynamics*; Cambridge University Press: **2005**.

103. Herschbach, D. R. Reactive Collisions in Crossed Molecular Beams. *Discuss. Faraday Soc.* **1962,** *33*, 149-161.

104. Grice, R.; Smith, D. Angular Distributions of Reactive Scattering Arising from Persistent Complexes with Dissociation at Arbitrary Angles to the Inertial Axes of the Transition State. *Mol. Phys.* **1993,** *80*, 1533-1540.

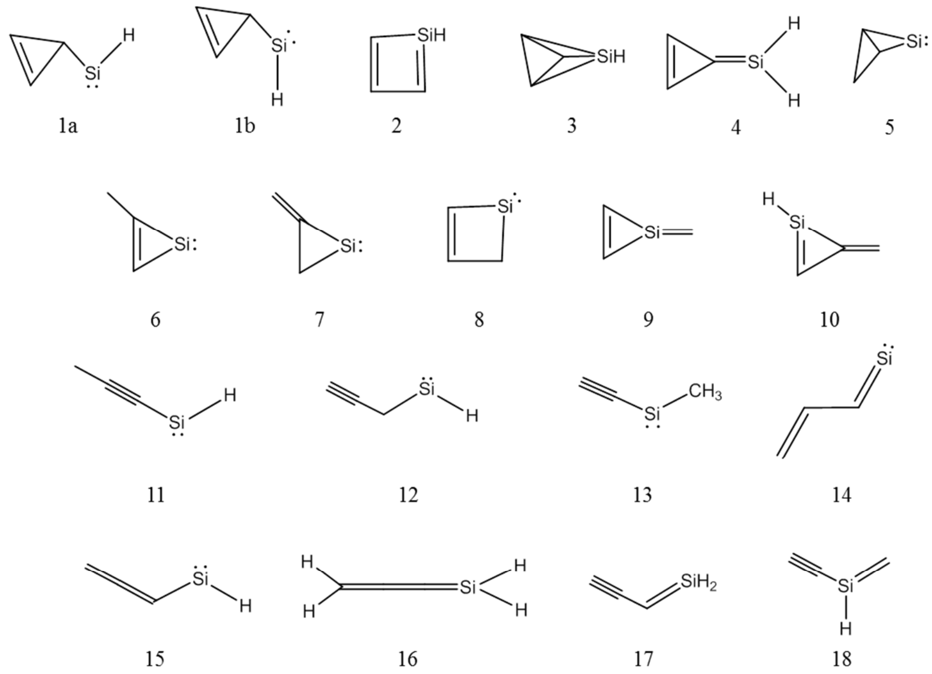

Figure 1. Compilation of the results of previous ab inito calculations on SiC_3H_4 isomers. They are the parent cyclopropenylsilylene (1a and 1b), silacyclobutadiene (2), silatetrahedrane (3), silylidenecyclopropene (4), 2-silabicyclo[1.1.0]butanylidene (5), 2-methyl-l-silacycloprop-2-en-l-ylidene (6), 2-methylenesilacycloprop-1-ylidene (7), silacyclobut-2-en-1-ylidene (8), 1-silamethylenecyclo-propene (9), 2-silamethylenecyclopropene (10), 1-propynylsilylene (11), 2-propynylsilylene (12), methylethynylsilylene (13), l-sila-l-buta-l,3-dienyldiene (14), 1,2-propadienylsilylene (15), 1-silabutatriene (16), 1-silabut-l-en-3-yne (17) and 2-silabut-l-en-3-yne (18). [Schriver, G. W.; Fink, M. J.; Gordon, M. S. Ab initio Calculations on Some C_3SiH_4 Isomers. *Organometallics* **1987**, *6*, 1977-1984].

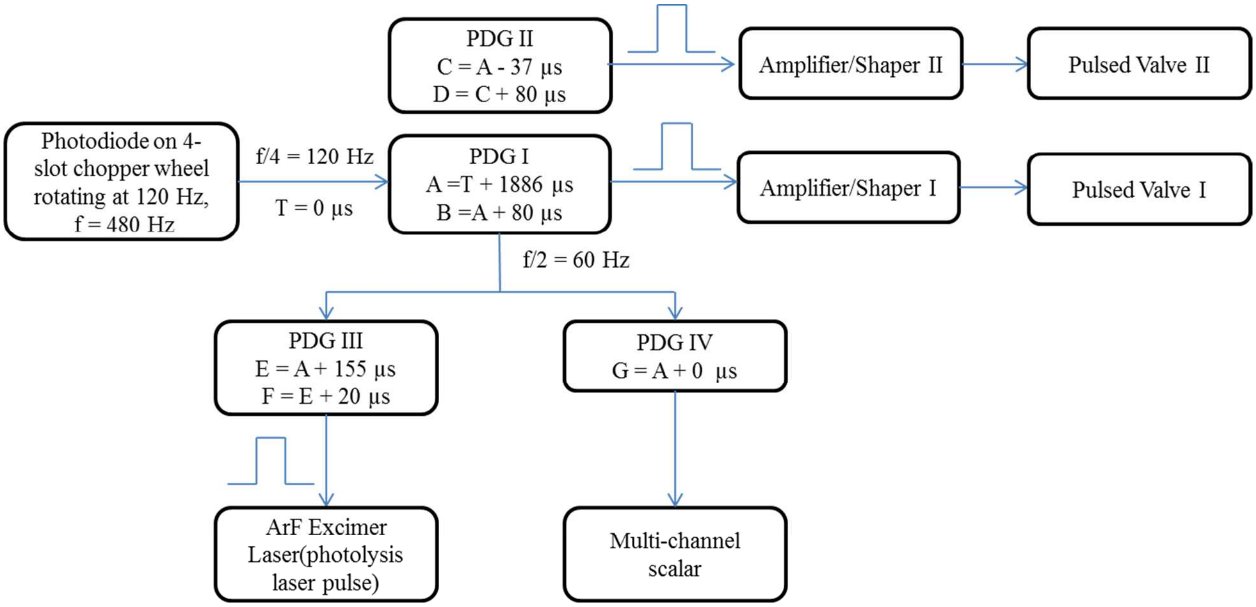

Figure 2. Pulse sequence for the crossed molecular beam experiment of the silylidyne radical (SiH; $X^2\Pi$) with allene (H_2CCCH_2; X^1A_1) and with D4-allene (D_2CCCD_2; X^1A_1). PDG: pulse/delay generator.

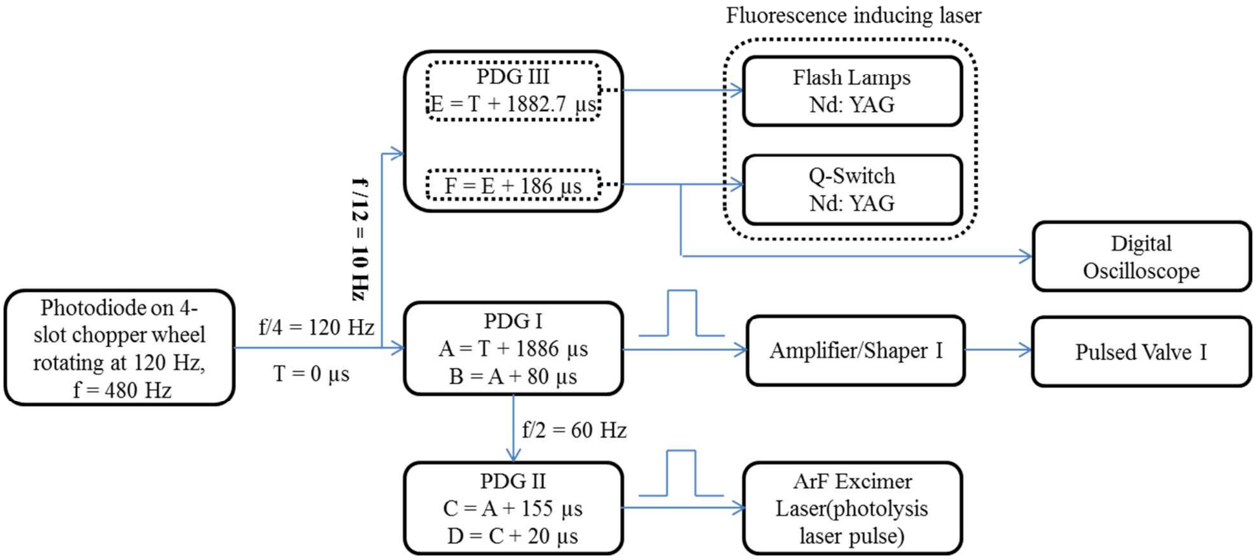

Figure 3. Pulse sequence for the laser induced fluorescence detection of the silylidyne radical (SiH; $X^2\Pi$).

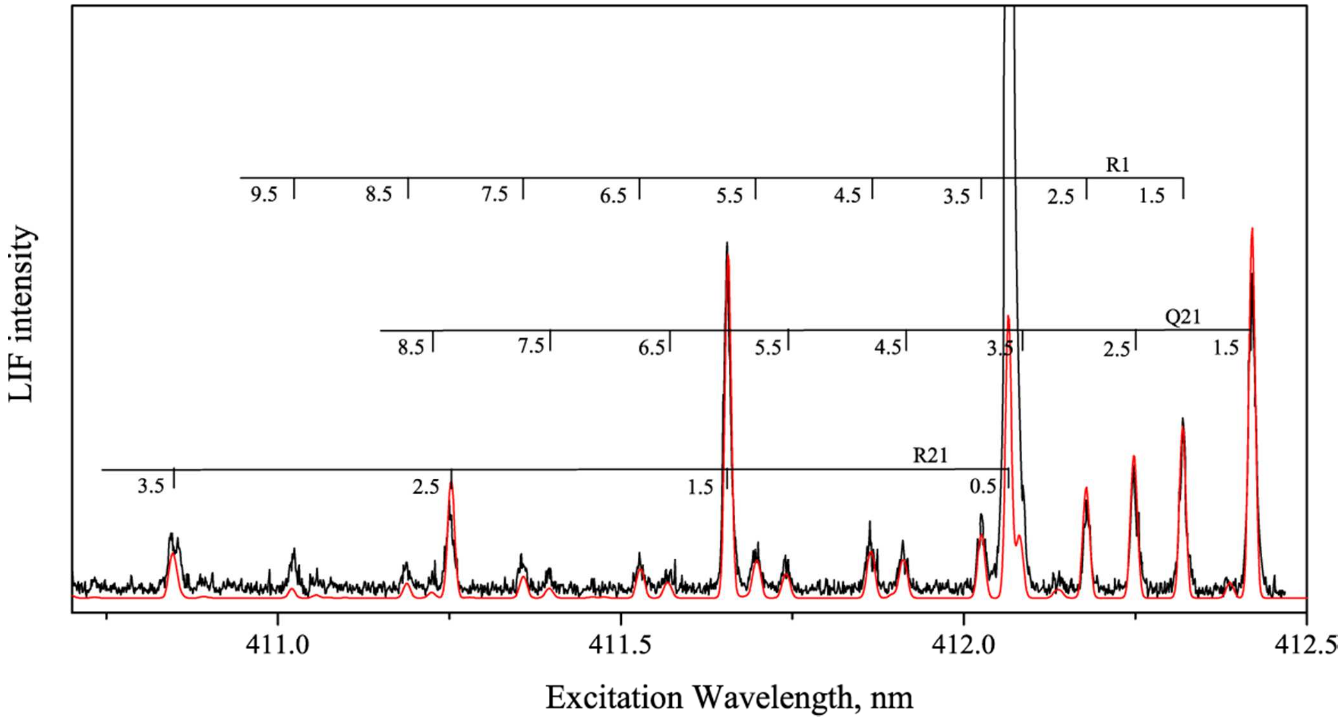

Figure 4. The SiH $A^2\Delta \leftarrow X^2\Pi$ excitation spectrum employed to determine the rotational temperature of the ground vibrational state. Simulation (red curve) suggests two silylidyne radical ensembles (see text for full details).

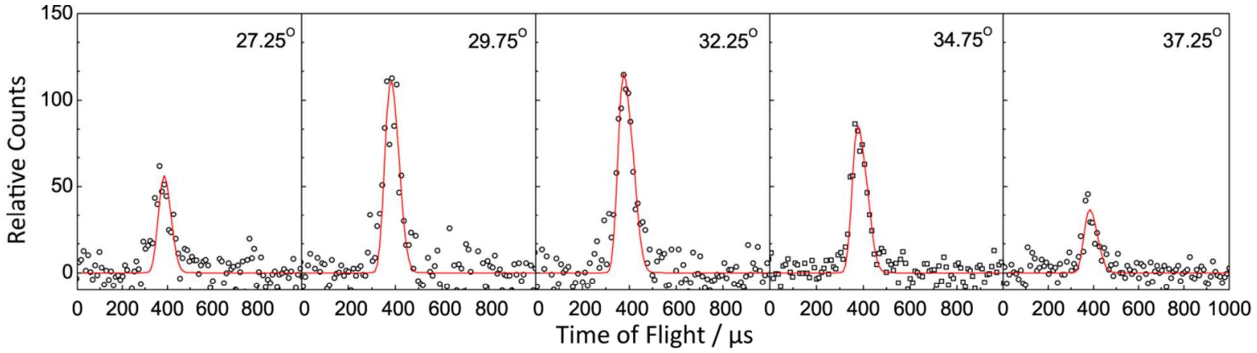

Figure 5. Selected time-of-flight (TOF) spectra recorded at a mass-to-charge ratio (*m/z*) of 68 ($SiC_3H_4^+$) for the reaction of the silylidyne radical (SiH; $X^2\Pi$) with allene (H_2CCCH_2; X^1A_1). The circles represent the experimental data, while the solid lines represent the best fits obtained from the forward-convolution routine.

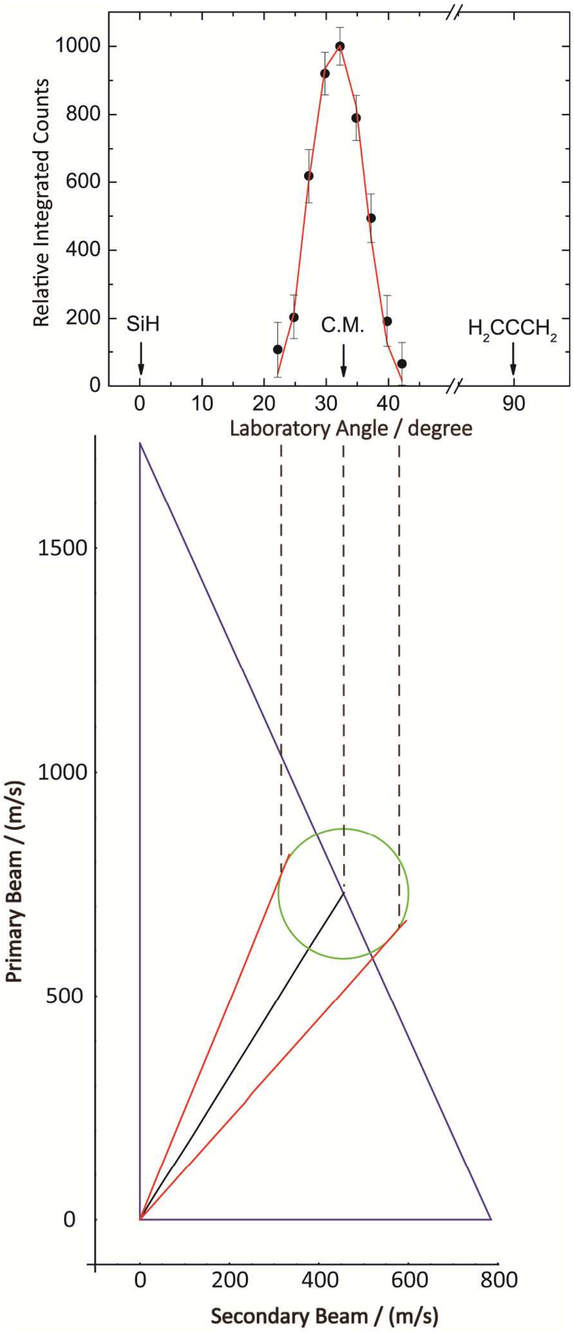

Figure 6. Laboratory angular distribution obtained at mass-to-charge ratio (*m/z*) of 68 for the reaction of the silylidyne radical (SiH; $X^2\Pi$) with allene (H_2CCCH_2; X^1A_1) (top) along with the most probable Newton diagram leading to SiC_3H_4 plus atomic hydrogen (bottom). In the angular distribution, the circles represent the experimental data, while the solid lines represent the fits obtained from the forward-convolution routine. In the Newton diagram, the two red lines define the angular range while the central black indicates the center-of-mass angle.

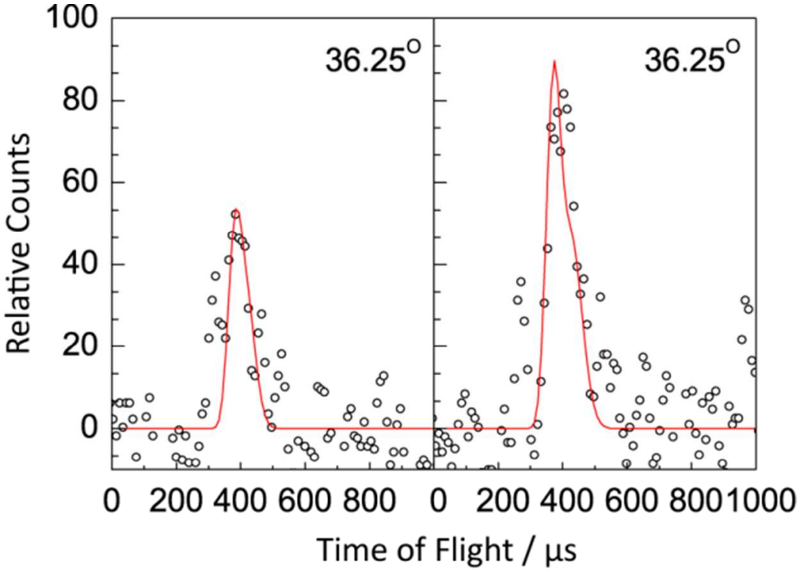

Figure 7. The center-of-mass TOF spectra for the reaction of the silylidyne radical (SiH; $X^2\Pi$) with D4-allene (D_2CCCD_2; X^1A_1) for the atomic hydrogen loss ($SiC_3D_4^+$, $m/z = 72$, left) and the atomic deuterium loss channel ($SiC_3D_3H^+$, $m/z = 71$, right), respectively.

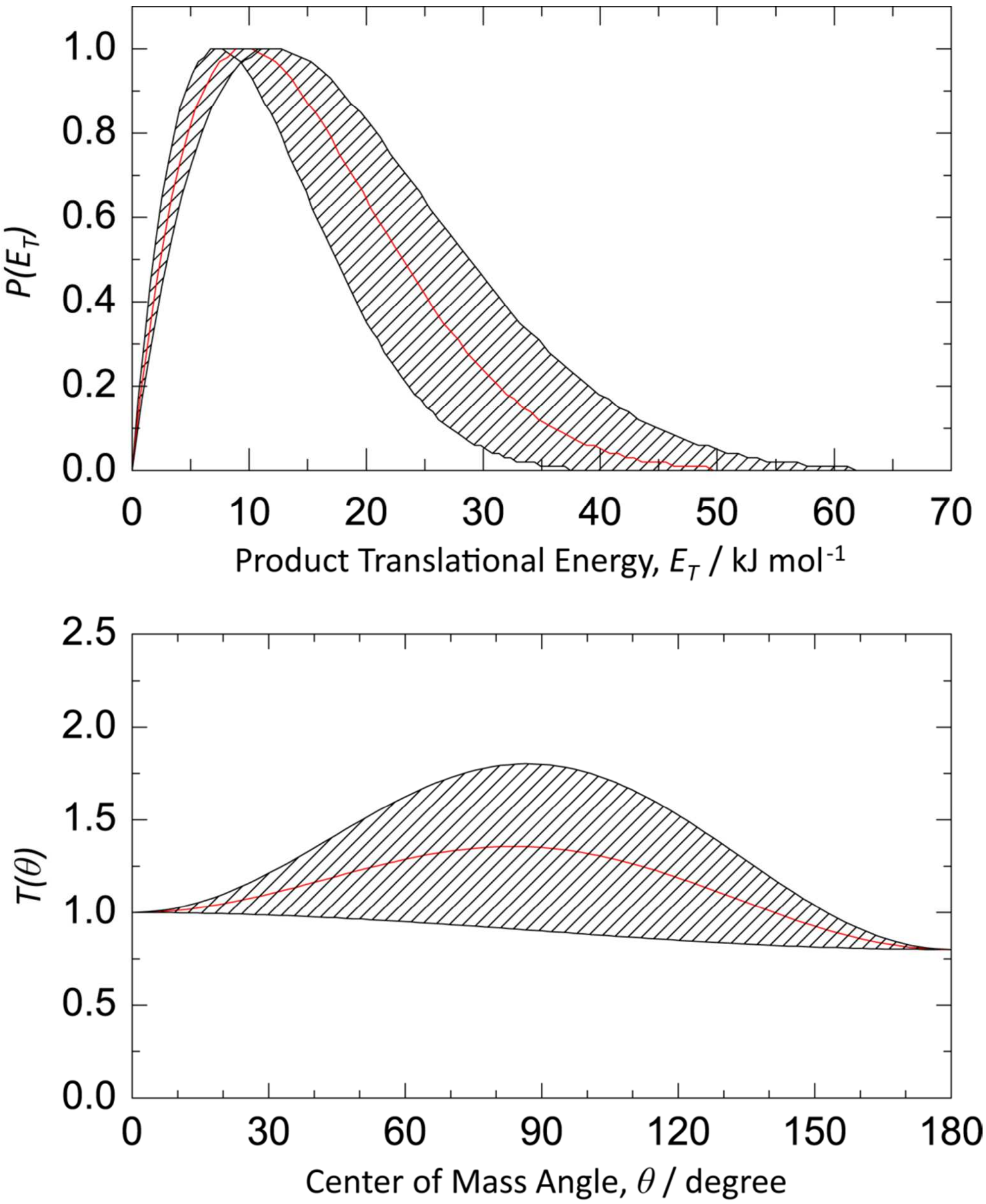

Figure 8. Center-of-mass translational energy distribution $P(E_T)$ (top) and angular distribution $T(\theta)$ (bottom) for the reaction of the silylidyne radical with allene forming SiC_3H_4 isomer(s). The hatched areas account for the error limits.

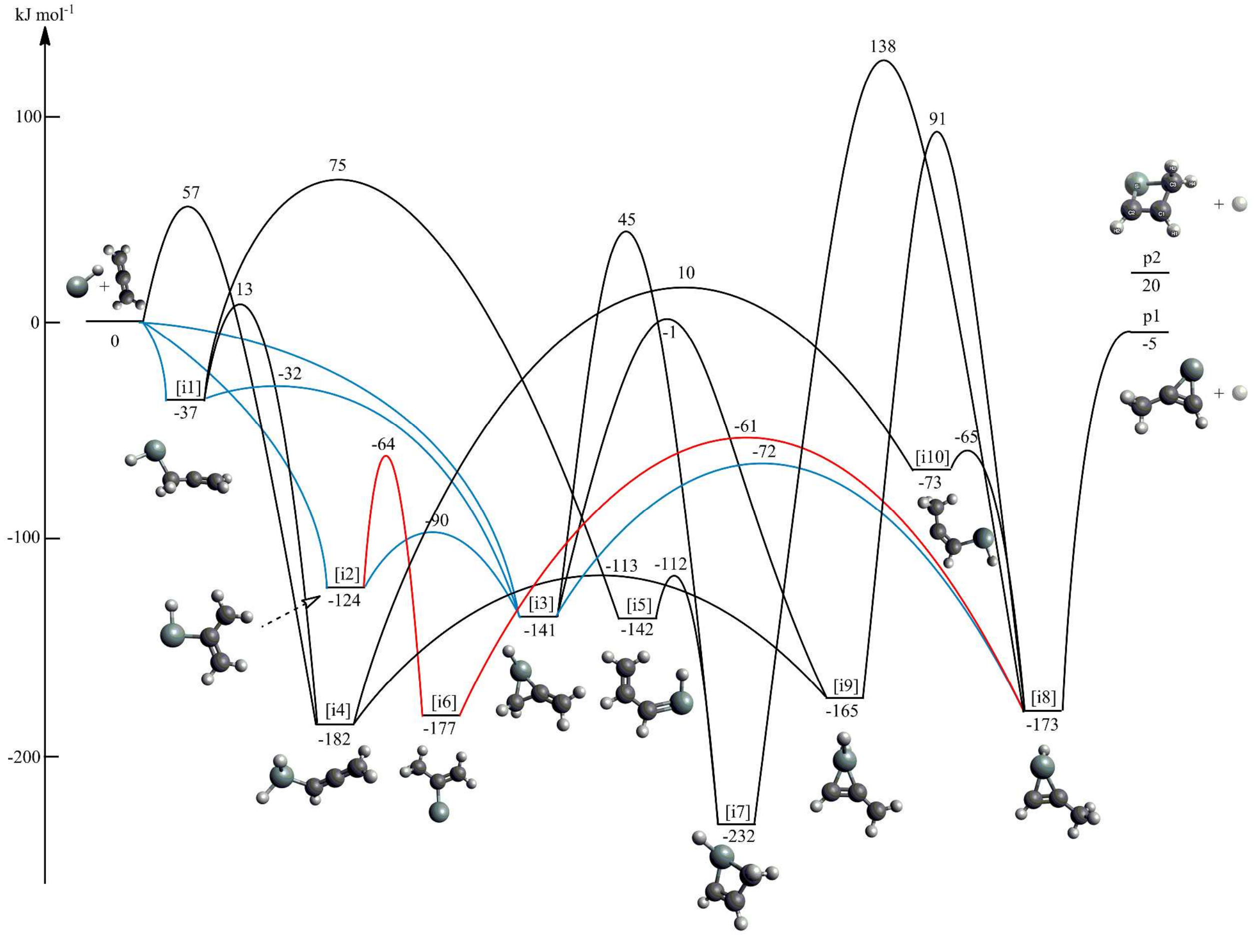

Figure 9. Relevant stationary points of the SiC_3H_5 potential energy surface for the reaction of the silylidyne radical (SiH; $X^2\Pi$) with allene (H_2CCCH_2; X^1A_1). Energies of the intermediates, transition states, and products are given relative to the reactants energy in kJ mol^{-1}. The elucidated reaction pathways 1 and 2 are denoted in blue and red, respectively, while black lines indicate pathways that are closed under the experimental reaction conditions.

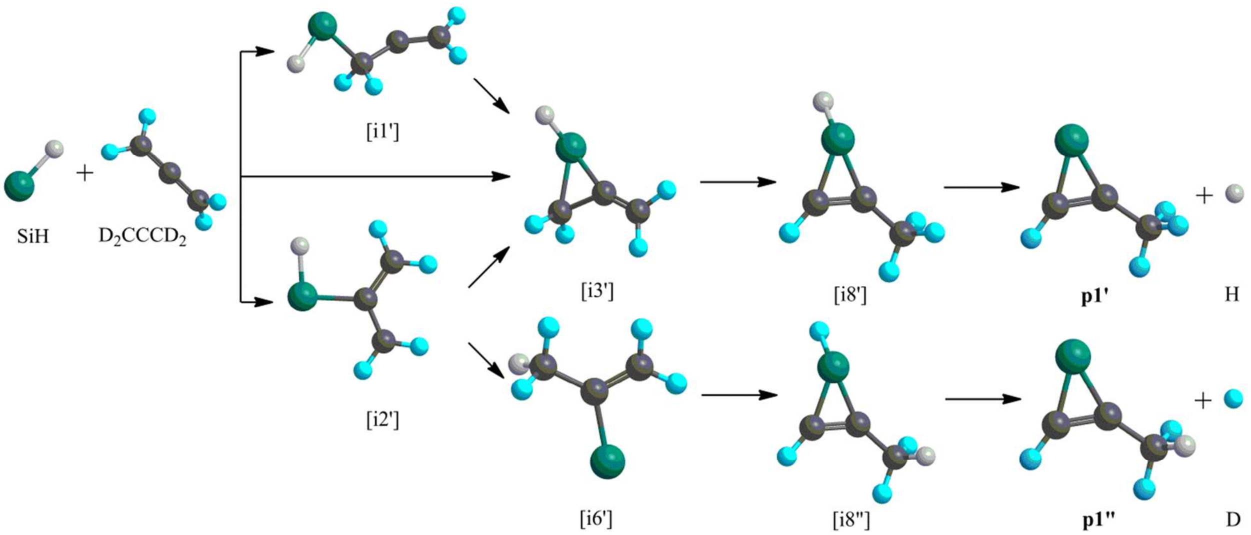

Figure 10. Reaction pathways from the initial collision complexes [i1’], [i2’] and [i3’] leading to two decomposing intermediates [i8’] and [i8”], which result in the formation on two distinct products **p1’** and **p1”**, respectively, via hydrogen loss and a deuterium loss, respectively.

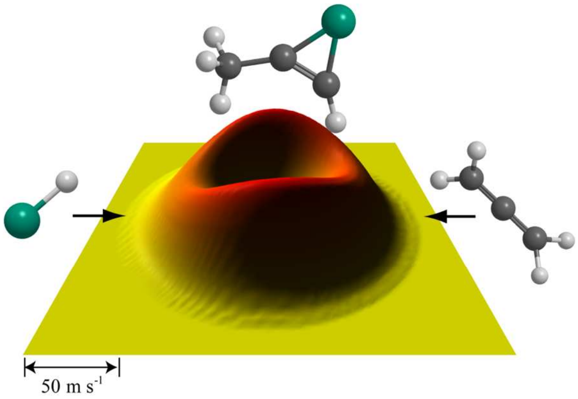

TOC Figure. Flux contour map for the reaction of the silylidyne radical (SiH; $X^2\Pi$) with allene (H_2CCCH_2; X^1A_1) yielding 2-methyl-1-silacycloprop-2-enylidene molecule (SiC_3H_4).

Table 1. Structures of the reactants, products, intermediates, and transition states calculated at the ωB97X-V/cc-pVTZ level of theory. Energies relative to the reactants are given in kJ mol^{-1}. Energies marked with "*" were obtained via CCSD(T)/CBS calculations. The point groups and symmetries of electronic wave functions are also included. Dark grey: carbon; blue grey: silicon; white: hydrogen.

Name	Relative Energy (kJ mol^{-1})	Point group and Symmetry of electronic wave function	Structure
SiH	0	$C_{\infty v} - {}^2\Pi$	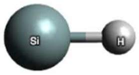
H_2CCCH_2		$D_{2d} - {}^1A_1$	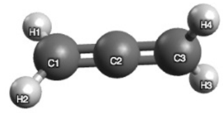
[p1]	-4.90*	$C_s - {}^1A'$	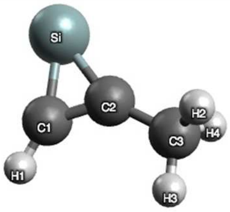
[p2]	20.2*	$C_1 - {}^1A$	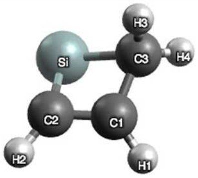
[i1]	-36.6	$C_1 - {}^2A$	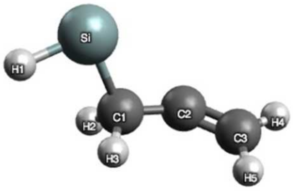
[i2]	-124.2	$C_s - {}^2A'$	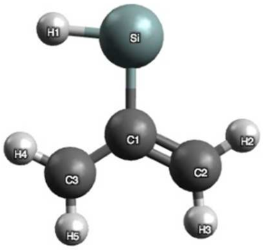

[i3]	-140.9	$C_1 – {}^2A$	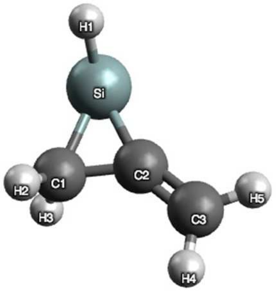
[i4]	-182.5	$C_1 – {}^2A$	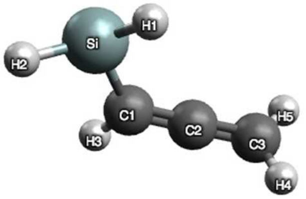
[i5]	-141.5	$C_s – {}^2A'$	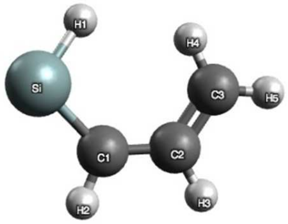
[i6]	-176.6	$C_s – {}^2A'$	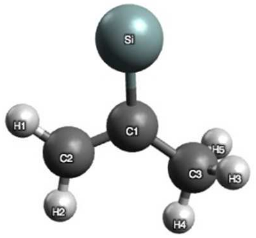
[i7]	-232.4	$C_1 – {}^2A$	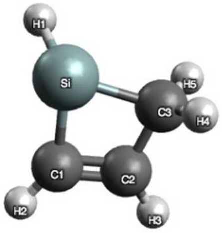
[i8]	-172.6	$C_1 – {}^2A$	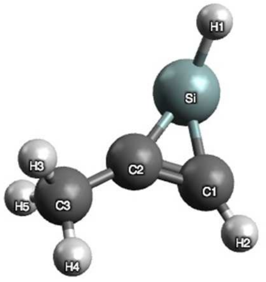

[i9]	-165.4	$C_s - {}^2A'$	
[i10]	-73.0	$C_s - {}^2A'$	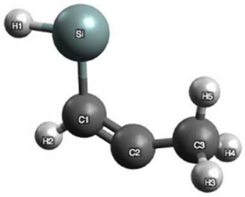
[r-i4]	57.0	$C_1 - {}^2A$	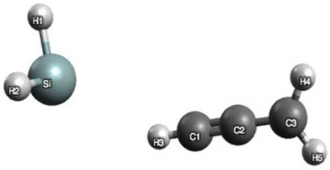
[i1-i3]	-31.8	$C_1 - {}^2A$	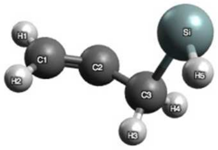
[i1-i4]	13.0	$C_1 - {}^2A$	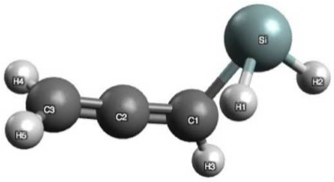
[i1-i5]	75.2	$C_1 - {}^2A$	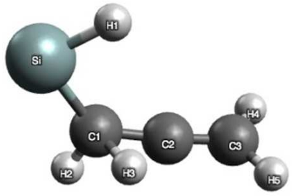
[i2-i3]	-89.6	$C_1 - {}^2A$	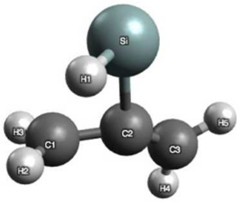
[i2-i6]	-64.0	$C_1 - {}^2A$	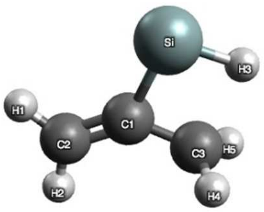

[i3-i7]	45.2	$C_1 - {}^2A$	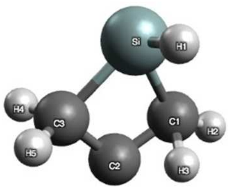
[i3-i8]	-72.3	$C_1 - {}^2A$	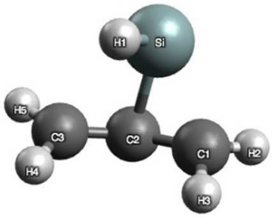
[i3-i9]	-1.0	$C_1 - {}^2A$	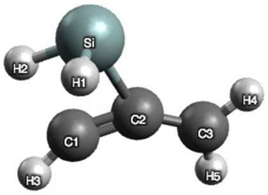
[i4-i9]	-113.4	$C_s - {}^2A'$	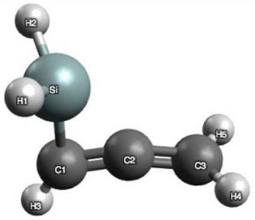
[i4-i10]	10.1	$C_1 - {}^2A$	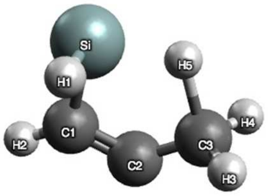
[i5-i7]	-112.2	$C_1 - {}^2A$	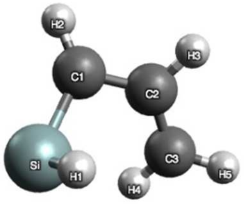
[i6-i8]	-61.2	$C_1 - {}^2A$	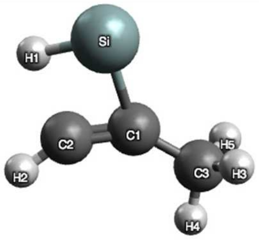

[i7-i8]	137.7	$C_1 - {}^2A$	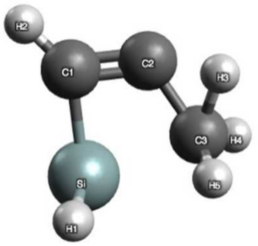
[i8-i9]	90.7	$C_1 - {}^2A$	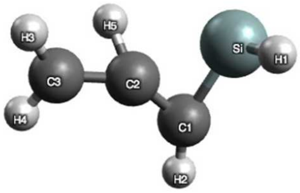
[i8-i10]	-64.7	$C_1 - {}^2A$	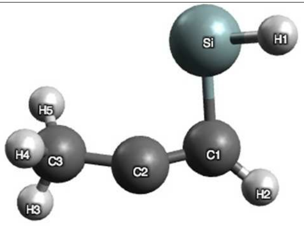

Table 2. Bond lengths and angles of the reactants, products, intermediates, and transition states calculated at the ωB97X-V/cc-pVTZ level of theory. Bond lengths are reported in picometers and angles in degrees.

Reactants		
H_2CCCH_2	$r(C_1,C_2)$	130.2
	$r(C_1,H_1)$	108.5
	$\theta(C_2,C_1,H_1)$	120.9°
SiH	$r(Si,H)$	152.9
Products		
[p1]	$r(Si,C_1)$	181.4
	$r(Si,C_2)$	182.7
	$r(C_1,C_2)$	134.3
	$r(C_2,C_3)$	148.8
	$r(C_1,H_1)$	108.5
	$r(C_3,H_2)$	109.3
	$\theta(Si,C_1,C_2)$	68.9°
	$\theta(C_1,C_2,C_3)$	137.0°
[p2]	$r(Si,C_2)$	183.3
	$r(Si,C_3)$	197.1
	$r(C_1,C_2)$	136.9
	$r(C_1,C_3)$	148.4
	$r(C_1,H_1)$	109.3
	$r(C_2,H_2)$	108.3
	$r(C_3,H_3)$	108.7
	$\theta(Si,C_2,C_1)$	84.8°
	$\theta(Si,C_3,C_1)$	77.1°
	$\theta(C_2,Si,C_3)$	75.3°
	$\theta(C_2,C_1,C_3)$	109.2°
Intermediates		
[i1]	$r(Si,C_1)$	192.0
	$r(Si,H_1)$	152.9
[i3]	$r(Si,C_1)$	187.8
	$r(Si,C_2)$	182.0
	$r(Si,H_1)$	149.5
	$r(C_1,C_2)$	153.1
	$r(C_2,C_3)$	132.1
	$r(C_1,H_2)$	108.9
	$r(C_3,H_4)$	108.8
	$\theta(Si,C_1,C_2)$	63.6°
	$\theta(C_1,C_2,C_3)$	135.3°
[i4]	$r(Si,C_1)$	185.7
	$r(Si,H_1)$	148.8
	$r(C_1,C_2)$	130.9
	$r(C_2,C_3)$	130.2
	$r(C_1,H_3)$	108.8
	$r(C_3,H_4)$	108.5
	$\theta(Si,C_1,C_2)$	121.6°
	$\theta(H_1,Si,H_2)$	111.6°
[i5]	$r(Si,C_1)$	185.7
	$r(Si,H_1)$	152.5
	$r(C_1,C_2)$	141.9
	$r(C_2,C_3)$	136.4
	$r(C_1,H_2)$	109.1
	$r(C_2,H_3)$	109.0
	$r(C_3,H_4)$	108.3
	$\theta(Si,C_1,C_2)$	130.6°
	$\theta(C_1,C_2,C_3)$	126.1°
[i6]	$r(Si,C_1)$	186.4
	$r(C_1,C_2)$	134.7

	r(C_1,C_2)	146.4
	r(C_2,C_3)	130.7
	r(C_1,H_2)	110.0
	r(C_3,H_4)	108.6
	θ(Si,C_1,C_2)	115.2°
	θ(C_1,C_2,C_3)	141.2°
[i2]	r(Si,C_1)	189.9
	r(Si,H_1)	152.7
	r(C_1,C_2)	139.1
	r(C_1,C_3)	139.4
	r(C_2,H_2)	108.5
	r(C_3,H_4)	108.3
	θ(Si,C_1,C_3)	122.9°
	θ(C_2,C_1,C_3)	121.3°
	r(C_1,C_3)	150.7
	r(C_2,H_1)	108.9
	r(C_3,H_3)	109.3
	θ(Si,C_1,C_2)	108.9°
	θ(C_2,C_1,C_3)	121.7°
[i7]	r(Si,C_1)	186.0
	r(Si,C_3)	191.5
	r(Si,H_1)	150.0
	r(C_1,C_2)	134.5
	r(C_2,C_3)	152.4
	r(C_1,H_2)	108.2
	r(C_2,H_3)	109.1
	r(C_3,H_4)	109.2
	θ(Si,C_1,C_2)	90.4°
	θ(Si,C_3,C_2)	83.2°
	θ(C_1,Si,C_3)	76.8°
	θ(C_1,C_2,C_3)	109.6°
[i8]	r(Si,C_1)	181.2
	r(Si,C_2)	182.3
	r(Si,H_1)	150.9
	r(C_1,C_2)	134.1
	r(C_2,C_3)	148.7
	r(C_1,H_2)	108.4
	r(C_3,H_3)	109.3
	θ(Si,C_1,C_2)	68.8°
	θ(C_1,C_2,C_3)	136.9°
[i9]	r(Si,C_1)	181.1
	r(Si,C_2)	182.7
	r(Si,H_1)	148.4
	r(C_1,C_2)	137.3
	r(C_1,H_1)	108.6
	r(C_3,H_4)	109.9
	θ(Si,C_3,C_2)	106.5°
	θ(C_1,C_2,C_3)	140.2°
[i1-i4]	r(Si,C_1)	192.3
	r(Si,H_1)	161.2
	r(Si,H_2)	151.7
	r(C_1,C_2)	133.9
	r(C_2,C_3)	129.8
	r(C_1,H_1)	160.4
	r(C_1,H_3)	108.8
	r(C_3,H_4)	108.6
	θ(Si,C_1,C_2)	121.5°
	θ(C_1,Si,H_1)	53.1°
[i1-i5]	r(Si,C_1)	190.4
	r(Si,H_1)	153.1

	r(C_2,C_3)	139.0
	r(C_1,H_3)	108.3
	r(C_3,H_4)	108.3
	θ(Si,C_1,C_2)	68.5°
	θ(C_1,C_2,C_3)	137.1°
	θ(H_1,Si,H_2)	111.3°
[i10]	r(Si,C_1)	188.3
	r(Si,H_1)	152.7
	r(C_1,C_2)	131.9
	r(C_2,C_3)	147.0
	r(C_1,H_2)	109.0
	r(C_3,H_3)	109.3
	θ(Si,C_1,C_2)	118.2°
	θ(C_1,C_2,C_3)	139.9°
	Transition States	
[r-i4]	r(Si,C_1)	407.1
	r(Si,H_1)	152.2
	r(C_1,C_2)	121.9
	r(C_2,C_3)	137.3
	r(C_1,H_3)	106.6
	r(C_3,H_4)	108.3
	θ(Si,C_1,C_2)	138.8°
	θ(H_1,Si,H_2)	92.4°
[i1-i3]	r(Si,C_3)	193.4
	r(Si,C_2)	273.9
	r(Si,H_5)	153.0
	r(C_1,C_2)	131.0
	r(C_2,C_3)	146.8
	r(C_1,C_2)	139.5
	r(C_2,C_3)	130.0
	r(C_1,H_2)	109.2
	r(C_1,H_3)	124.4
	r(C_2,H_3)	138.1
	r(C_3,H_4)	108.9
	θ(Si,C_1,C_2)	129.5°
	θ(C_1,C_2,C_3)	175.5°
	θ(C_2,C_1,H_3)	62.8°
[i2-i3]	r(Si,C_1)	238.5
	r(Si,C_2)	192.6
	r(Si,H_1)	151.9
	r(C_1,C_2)	140.3
	r(C_2,C_3)	133.7
	r(C_1,H_2)	108.2
	r(C_3,H_4)	108.7
	θ(Si,C_2,C_1)	90.1°
	θ(Si,C_2,C_3)	128.6°
	θ(C_1,C_2,C_3)	137.4°
[i2-i6]	r(Si,C_1)	189.9
	r(Si,H_3)	155.2
	r(C_1,C_2)	133.0
	r(C_1,C_3)	142.1
	r(C_2,H_1)	108.4
	r(C_3,H_3)	180.6
	r(C_3,H_4)	108.7
	θ(Si,C_1,C_3)	84.1°
	θ(C_2,C_1,C_3)	138.7°

[i3-i7]	r(Si,C_1)	193.5
[i4-i10]	r(Si,C_1)	193.2

	r(Si,C_3)	194.4
	r(Si,H_1)	151.3
	r(C_1,C_2)	140.9
	r(C_2,C_3)	151.0
	r(C_1,H_2)	108.7
	r(C_1,H_3)	121.6
	r(C_2,H_3)	142.4
	r(C_3,H_4)	109.5
	θ(Si,C_1,C_2)	92.1°
	θ(Si,C_3,C_2)	88.8°
	θ(C_1,Si,C_3)	73.6°
	θ(C_1,C_2,C_3)	105.4°
	θ(C_2,C_1,H_3)	65.2°
[i3-i8]	r(Si,C_1)	198.7
	r(Si,C_2)	191.3
	r(Si,H_1)	151.3
	r(C_1,C_2)	144.5
	r(C_2,C_3)	135.3
	r(C_1,H_2)	108.5
	r(C_3,H_4)	109.2
	θ(Si,C_2,C_1)	71.0°
	θ(Si,C_2,C_3)	99.2°
	θ(C_1,C_2,C_3)	126.6°
[i3-i9]	r(Si,C_1)	211.7
	r(Si,C_2)	196.6
	r(Si,H_1)	151.5
	r(C_1,C_2)	129.9
	r(C_2,C_3)	137.8
	r(C_1,H_2)	171.7
	r(C_1,H_3)	107.4
	r(C_3,H_4)	108.2
	r(Si,H_1)	151.5
	r(Si,H_5)	165.5
	r(C_1,C_2)	130.4
	r(C_2,C_3)	139.4
	r(C_1,H_2)	108.3
	r(C_3,H_3)	108.9
	r(C_3,H_5)	148.9
	θ(Si,C_1,C_2)	102.5°
	θ(C_1,C_2,C_3)	127.0°
	θ(H_1,Si,H_5)	102.4°
[i5-i7]	r(Si,C_1)	183.3
	r(Si,C_3)	279.5
	r(Si,H_1)	151.6
	r(C_1,C_2)	142.9
	r(C_2,C_3)	135.8
	r(C_1,H_2)	108.4
	r(C_2,H_3)	109.2
	r(C_3,H_4)	108.6
	θ(Si,C_1,C_2)	104.0°
	θ(C_1,C_2,C_3)	121.9°
[i6-i8]	r(Si,C_1)	194.1
	r(Si,C_2)	212.3
	r(Si,H_1)	155.5
	r(C_1,C_2)	127.7
	r(C_1,C_3)	148.6
	r(C_2,H_1)	170.7
	r(C_2,H_2)	107.6
	r(C_3,H_3)	109.3
	θ(Si,C_1,C_2)	79.7°
	θ(C_1,C_2,C_3)	143.1°
[i7-i8]	r(Si,C_1)	190.5

	$\theta(\mathrm{Si,C_2,C_1})$	77.9°
	$\theta(\mathrm{C_1,C_2,C_3})$	146.2°
	$\theta(\mathrm{H_1,Si,H_2})$	101.5°
[i4-i9]	$r(\mathrm{Si,C_1})$	181.9
	$r(\mathrm{Si,C_2})$	210.0
	$r(\mathrm{Si,H_1})$	148.4
	$r(\mathrm{C_1,C_2})$	131.2
	$r(\mathrm{C_2,C_3})$	135.8
	$r(\mathrm{C_1,H_3})$	108.4
	$r(\mathrm{C_3,H_4})$	108.3
	$\theta(\mathrm{Si,C_1,C_2})$	82.5°
	$\theta(\mathrm{C_1,C_2,C_3})$	164.2°

	$r(\mathrm{Si,C_2})$	230.0
	$r(\mathrm{Si,C_3})$	212.6
	$r(\mathrm{Si,H_1})$	153.3
	$r(\mathrm{C_1,C_2})$	131.9
	$r(\mathrm{C_2,C_3})$	155.0
	$r(\mathrm{C_1,H_2})$	108.1
	$r(\mathrm{C_2,H_3})$	131.9
	$r(\mathrm{C_3,H_3})$	126.1
	$r(\mathrm{C_3,H_4})$	108.2
	$\theta(\mathrm{Si,C_1,C_2})$	89.1°
	$\theta(\mathrm{Si,C_3,C_2})$	75.7°
	$\theta(\mathrm{C_1,Si,C_3})$	75.3°

	$\theta(\mathrm{C_1,C_2,C_3})$	118.5°
	$\theta(\mathrm{C_2,C_3,H_3})$	54.8°
[i8-i9]	$r(\mathrm{Si,C_1})$	178.3
	$r(\mathrm{Si,C_2})$	197.3
	$r(\mathrm{Si,H_1})$	151.7
	$r(\mathrm{Si,H_5})$	234.4
	$r(\mathrm{C_1,C_2})$	139.5
	$r(\mathrm{C_2,C_3})$	139.0
	$r(\mathrm{C_1,H_2})$	108.1
	$r(\mathrm{C_2,H_5})$	119.8
	$r(\mathrm{C_3,H_3})$	108.4
	$r(\mathrm{C_3,H_5})$	149.8
	$\theta(\mathrm{Si,C_1,C_2})$	75.7°
	$\theta(\mathrm{C_1,C_2,C_3})$	141.0°
	$\theta(\mathrm{C_3,C_2,H_5})$	70.3°
[i8-i10]	$r(\mathrm{Si,C_1})$	188.5
	$r(\mathrm{Si,C_2})$	242.8

r(Si,H_1)	153.1
r(C_1,C_2)	130.0
r(C_2,C_3)	146.5
r(C_1,H_2)	108.9
r(C_3,H_3)	109.5
θ(Si,C_1,C_2)	97.7°
θ(C_1,C_2,C_3)	155.8°

Table 3. NICS values for **p1**, c-SiC_2H_2, and c-$C_3H_3^+$ calculated at the HF/cc-pVDZ and B3LYP/cc-pVDZ.

	NICS Value	
	HF	B3LYP
p1	-21.638	-17.595
c-SiC_2H_2	-19.851	-15.682
c-$C_3H_3^+$	-28.621	-23.257